

Euphotic zone metabolism in the North Pacific Subtropical Gyre based on oxygen dynamics

Sara Ferrón^{*1}, Benedetto Barone¹, Matthew J. Church², Angelicque E. White¹, and David M. Karl¹

¹Daniel K. Inouye Center for Microbial Oceanography: Research and Education, Department of Oceanography, School of Ocean and Earth Science and Technology, University of Hawaii at Manoa, 1950 East-West Road, Honolulu, Hawaii 96822, USA

²Flathead Lake Biological Station, University of Montana, Polson, Montana 59860, USA

*Corresponding author:

Tel: +1-808-956-3420. Email: sferron@hawaii.edu

Keypoints

- Time-series measurements (>5 years) of mixed layer O₂/Ar in the oligotrophic ocean show consistent diel cycles
- There is pronounced seasonality in euphotic zone net community production rates, with maxima in May and minima in December
- Annual net community production in the euphotic zone exceeds C export through sinking particles by ~2-fold

ABSTRACT

We report in situ rates of gross oxygen production (GOP), community respiration (R), and net community production (NCP) in the North Pacific Subtropical Gyre derived from mixed layer O₂/Ar measurements. The measurements were conducted between November 2013 and January 2019 at the site of the Hawaii Ocean Time-series program. Biological O₂ concentration anomalies in the mixed layer showed a consistent diel variation, with values increasing during daytime due to net primary production and decreasing during nighttime due to respiration. In situ mixed layer GOP and R, determined from these variations, co-varied but showed no clear seasonal pattern, averaging 0.9 and 0.8 mmol O₂ m⁻³ d⁻¹, respectively. In situ rates of NCP determined from mixed layer O₂/Ar ranged between -0.7 and 17.6 mmol O₂ m⁻² d⁻¹. Our analyses indicate that at certain times of the year the diapycnal flux of O₂ across the base of the mixed layer may be non-negligible and therefore a fraction of O₂/Ar-derived NCP may form below the mixed layer. The seasonal climatology of NCP below the mixed layer (down to 150 m) was also estimated using near-monthly changes in dissolved O₂ concentrations. These calculations allowed us to estimate NCP for the entire euphotic zone (0-150 m), which shows pronounced seasonality, with a maximum in May and a minimum in December, when the ecosystem becomes temporarily net heterotrophic. Annual NCP was estimated to be 2.4 ± 0.5 mol O₂ m⁻² yr⁻¹, approximately twice the export of C through sinking particles captured in sediment traps at 150 m.

1. Introduction

Oceanic primary production, primarily through oxygenic photosynthesis, represents the main input of energy into marine ecosystems (Karl, 2014), is the first step of the ocean's food web (Ryther, 1969), and produces approximately half of the oxygen (O_2) on the planet (Field et al., 1998). In addition, primary production in the ocean drives the marine biological carbon (C) pump that in turns affects climate (Volk & Hoffert, 1985). Planktonic primary production and respiration can be quantified in terms of energy or material flows (Williams, 1993), but the latter is operationally easier to measure. Therefore, gross primary production (GPP) is commonly defined as the total amount of inorganic C that is reduced to organic C by photosynthetic organisms (Williams, 1993). A large fraction of this C is oxidized back to carbon dioxide (CO_2) through community respiration (R) by both autotrophic and heterotrophic organisms. The difference between GPP and R, net community production (NCP), represents the amount of biologically produced organic C that can be potentially transported out of the euphotic zone into the ocean's interior via the biological C pump, mainly through sinking particles, vertically migrating zooplankton (Longhurst & Harrison, 1988), and the export of dissolved organic C (Carlson et al., 1994). Through these processes the biological C pump effectively sequesters CO_2 from the atmosphere for extended periods of time (Volk & Hoffert, 1985) and provides the main C source that fuels meso- and abyssopelagic organisms (Karl & Church, 2017).

The oligotrophic subtropical gyres occupy approximately 40% of the world's surface (Karl & Church, 2014) and because of their large areal extent they are important contributors to the oceanic biological C pump (Emerson, 2014; Emerson et al., 1997). However, quantifying metabolic rates in the subtropical oligotrophic gyres is challenging, mostly due to the low rates that characterize these regions of the ocean, the episodic non steady-state nature of these habitats, and the susceptibility of the microbial communities to small environmental perturbations introduced during incubation procedures (Williams et al., 2004). Proof of this difficulty is the clear discrepancy in NCP estimates from in vitro versus in situ geochemical mass balance methods that has generated much debate over the metabolic status of the surface oligotrophic ocean (e.g. Duarte et al., 2013; Ducklow & Doney, 2013; Williams et al., 2013). Accurate estimates of the biological C pump in subtropical oligotrophic gyres are therefore critical for constraining the oceanic C cycle, understanding the factors driving its temporal variability, and improving our capability to predict how ocean ecosystems will respond to climate change.

Because the production and consumption of O_2 are directly linked to GPP and R, O_2 has been frequently used as biochemical tracer of NCP and biological C fluxes (Emerson et al., 1995, 1997; Nicholson et al., 2008; Riser & Johnson, 2008; Yang et al., 2017). In the mixed layer, the concentration of dissolved O_2 is controlled by biological processes (GPP and R), air-water gas exchange (both through diffusive fluxes and bubble injection), as well as horizontal and vertical mixing and diffusion. Horizontal O_2 advection is thought to be small, so it is normally neglected (Emerson et al., 1997). In the North Pacific Subtropical Gyre (NPSG), diapycnal O_2 fluxes at the base of the mixed layer are often considered to be small (Nicholson et al., 2012; Quay et al., 2010), although recently Barone et al. (2019b) showed that they are non-negligible. Vertical fluxes associated with entrainment events due to the deepening of the mixed layer can potentially have a larger impact in the mixed layer O_2 budget, particularly if entrained waters have different dissolved O_2 concentration (Nicholson et al., 2012; Quay et al., 2010). In the absence of entrainment, a deviation of dissolved O_2 from equilibrium in the mixed layer can be due to either biological or physical processes. Physical processes include bubble injection through breaking waves, changes in solubility due to heating and cooling processes, and changes in atmospheric pressure (Hamme & Emerson, 2006). Because Ar is biologically inert but has physical properties similar to O_2 , the use of O_2 to Ar gas concentration ratios (hereafter O_2/Ar) eliminates the effects of physical processes so that the deviation of O_2/Ar from equilibrium is assumed to be primarily caused by biological processes (Craig & Hayward, 1987; Hamme & Emerson, 2006). When diffusive gas exchange, advection, and entrainment can be estimated or directly measured, in situ O_2/Ar have proven to be a reliable constraint on O_2 -based (e.g. Hamme & Emerson, 2006; Juranek & Quay, 2005; Kaiser et al., 2005; Luz & Barkan, 2009; Quay et al., 2010; Reuer et al., 2007). The air-sea flux of biological O_2 determined from O_2/Ar , under steady-state conditions, is equal to NCP over the residence time of O_2 in the mixed layer prior to the measurement (typically ~1-2 weeks). Recently, Teeter et al. (2018) demonstrated that on time scales longer than the mixed layer O_2 residence time, the air-sea flux of biological O_2 determined from O_2/Ar measurements represents the exponentially weighted average NCP, independent of whether the system is in steady-state or not.

In addition to being used as a time-integrative proxy of NCP, in situ mixed layer O_2/Ar collected over a diel cycle can be used to estimate rates of gross oxygen production (GOP) and O_2 consumption through R on shorter time scales (12-24 hours; Ferrón et al., 2015; Hamme et

al., 2012; Tortell et al., 2014). The diel O_2/Ar method relies on calculating net primary production from the net increase in O_2/Ar during daytime and R from the net decrease in O_2/Ar during the night, in both cases after a correction is made for gas exchange. In contrast to other in situ geochemical approaches, this method provides values that average over similar time scales as in vitro-derived rates. This might prove useful for comparing in vitro and in situ methods and determining whether the discrepancy between them might be due to episodic in time or heterogeneous in space processes that would be missed by the in vitro methods (Karl et al., 2003a; Williams et al., 2013).

Herein, we discuss the temporal variability of GOP, R, and NCP in the NPSG derived from in situ measurements of mixed layer O_2/Ar collected at near-monthly intervals over a period of >5 years. The samples were collected at the Hawaii Ocean Time-series (HOT) site, Station ALOHA (22°45'N, 158°00'W), located 100 km north of the island of Oahu, within the oligotrophic NPSG (Karl & Lukas, 1996). Established in 1988, Station ALOHA is one of the “few regions in the sea where we have sustained, decadal-scale observations on the interactions between ocean biogeochemistry, hydrography, and ecology” (Church et al., 2013). Core primary production measurements in the HOT program include dawn to dusk rates of ^{14}C -bicarbonate assimilation (^{14}C -PP) and sediment trap measurements of particulate matter export at 150 m. The former provide rates that represent values between net primary production (NPP, GPP minus autotrophic R) and GPP (Karl & Church, 2017). The latter provide measurements of particulate C flux from sinking particles, which is a fraction of export production (Boyd et al., 2019). As such, our study aims to contribute to the program by providing in situ rates of GOP, R, and NCP derived from O_2/Ar measurements. The temporal coverage of our measurements enables a determination of seasonal and interannual variability of metabolic rates and a quantitative estimation of annual NCP, a proxy for export production (Emerson, 2014) and arguably one of the most critical terms to understand the role of the ocean in regulating Earth’s climate.

2. Methods

2.1. Sample collection and analysis

Seawater samples were collected between November 2013 and January 2019 on 48 HOT cruises that were conducted at approximately monthly intervals. Seawater was collected using 12-L Niskin-type bottles attached to a CTD-rosette. The samples were transferred into 250 mL

borosilicate serum bottles using Tygon[®] tubing, filling from bottom to top, and allowing the water to overflow at least twice the volume of the bottle. Immediately after collection, samples were poisoned with 200 μ L of saturated mercuric chloride solution to inhibit biological activity, crimp sealed, and stored in the dark at room temperature until analysis, within 3-5 days of collection. For all HOT cruises, duplicate samples were collected every 3 hours at 25 m during a 24-hour period, to measure diel variability in O₂/Ar values (Ferrón et al., 2015). Starting in April 2015 (HOT cruise 271 and onward), as well as during the first cruise (November 2013, HOT 257), duplicate samples were also collected at 5 m.

Dissolved O₂/Ar molar ratios were measured in the lab by membrane-inlet mass spectrometry (MIMS) following Kana et al. (1994). The MIMS dissolved gas analyzer (Bay Instruments, Easton, Maryland) is described in detail by Ferrón et al. (2016). Briefly, the water sample is drawn at a constant flow (~ 2 mL min⁻¹) into a capillary tubing that passes through a 23.00 (± 0.01) °C water bath, to stabilize the sample temperature, and then through a 2.5 cm long semipermeable microbore silicone membrane (Silastic[®], DuPont) that is connected to a vacuum inlet system. As the sample flows through the membrane a fraction of the dissolved gases are extracted into the vacuum, pass through a cryo-trap that removes water vapor and CO₂, and enter a quadrupole mass spectrometer (HiQuad[™] QMG 700) equipped with a cross-beam ion source. A standard, consisting of 25 m filtered seawater (0.2 μ m) equilibrated with ambient air at 23.00 (± 0.01) °C, was run every ~ 30 minutes, to correct for instrument drift. Dissolved O₂ and Ar concentrations in the standard were calculated using the solubility equations reported by García and Gordon (1992) and Hamme and Emerson (2004), respectively. Based on the expected concentrations in the standard, calibration factors were calculated for every standard run and interpolated with time to correct for drift (Kana et al., 2006). The precision of duplicate samples (measured as the coefficient of variation) was on average 0.03% for O₂/Ar ratios.

2.2. Ancillary measurements from the HOT program

Since our sampling and subsequent measurements occurred as part of HOT cruises, a number of other biogeochemical parameters were available. The entire HOT dataset and measurement protocols are available at: <http://hahana.soest.hawaii.edu/hot/>.

Briefly, 14 to 15 vertical profiles of temperature, salinity, dissolved O₂, and chlorophyll fluorescence were collected at Station ALOHA during every HOT cruise during a 36-hour burst sampling period (Karl & Lukas, 1996). These measurements were collected using a conductivity, temperature, and depth (CTD) package (SBE911Plus, Sea-Bird), a Seapoint chlorophyll fluorometer, and a polarographic O₂ sensor (SBE43, Sea-Bird) attached to a rosette. The conductivity, O₂, and fluorescence sensors were calibrated with discrete samples following HOT procedures. Chlorophyll *a* and phaeopigments were measured fluorometrically and used to calibrate in situ fluorescence. Particle flux was measured using free floating sediment traps deployed at 150 m (Karl et al., 1996). Primary production was measured by the ¹⁴C-fixation method. Samples were incubated from dawn to dusk *in situ* at different depths (5, 25, 45, 75, 100, and 125 m), using a free floating array (Letelier et al., 1996). Depth-integrated (0-125 m) ¹⁴C-PP was obtained by applying the trapezoidal rule, and the uncertainty estimated by propagating the standard deviation (hereafter SD) of triplicate measurements at each depth.

The mixed layer depth was first calculated for each vertical profile as the first depth where the potential density was at least 0.03 kg m⁻³ larger than the value at 10 m (de Boyer Montégut et al., 2004). Then, for each cruise the largest potential density value at the base of the mixed layer was determined, and the cruise mixed layer depth was calculated as the mean depth of this isopycnal surface (as per Barone et al., 2019b).

2.3. NCP from mixed layer O₂/Ar mass balance

NCP (mmol O₂ m⁻² d⁻¹) in the mixed layer, NCP_{0-mld}, can be determined from the *in situ* O₂/Ar (Cassar et al., 2011; Craig & Hayward, 1987; Giesbrecht et al., 2012; Kaiser et al., 2005). The simplest approach assumes that, in the absence of vertical and horizontal mixing with other water masses, the net biological production of O₂ equals its flux to the atmosphere via gas exchange:

$$NCP_{0-mld} = k_w \Delta(O_2/Ar) [O_2]_{eq} \rho \quad (1)$$

where k_w is the weighted gas transfer velocity for O₂ (m d⁻¹, see below), $[O_2]_{eq}$ is the O₂ concentration at equilibrium with the atmosphere (mmol kg⁻¹), ρ is the density of seawater (kg m⁻³) in the mixed layer, and $\Delta(O_2/Ar)$ is the biological O₂ saturation anomaly, determined as:

$$\Delta(O_2/Ar) = \frac{(O_2/Ar)_{meas}}{(O_2/Ar)_{eq}} - 1 \quad (2)$$

where $(O_2/Ar)_{meas}$ and $(O_2/Ar)_{eq}$ are the measured O_2/Ar ratio and that expected at equilibrium with the atmosphere, respectively. $\Delta(O_2/Ar)$ represents the biological O_2 saturation anomaly.

The instantaneous gas transfer velocities for O_2 , k_{O_2} , were determined from wind speed measurements using the quadratic dependence reported by Wanninkhof (2014), which updates the widely used parameterization of Wanninkhof (1992). The Schmidt number for O_2 was calculated from the updated temperature-dependent equations reported by Wanninkhof (2014) for seawater. The uncertainty associated with k_{O_2} is approximately 20% (Wanninkhof, 2014). To calculate k_{O_2} we used wind speed measurements (1-minute temporal resolution) collected at 3.4 m above sea surface at the WHOI-Hawaii Ocean Time-Series (WHOTS) mooring (22° 45' N, 157° 55' W), available online at <http://uop.whoi.edu/projects/WHOTS/whotsdata.htm>. These data were scaled to estimate the wind speed at a height of 10 m above sea surface (Smith, 1988). Wind speed measurements from the WHOTS mooring were not available between August 2016 and April 2017. During that period, we used preliminary satellite estimates of wind speed at 10 m above the sea surface from microwave backscatter. These data were obtained from the Blended Sea Winds data product (Zhang et al., 2006), produced by the National Oceanic and Atmospheric Administration's National Climatic Data Center (NOAA-NCDC). Whereas the WHOTS wind speed data are 1-minute resolution measurements at a spot location within Station ALOHA, NOAA satellite-derived estimates of wind speed have an horizontal resolution of 0.25° in latitude and longitude (>25 km), and a temporal resolution of 6 hours. Despite this, 6-hour averages of WHOTS wind speed measurements were highly correlated with satellite-based estimates ($r^2 = 0.66$, $p < 10^{-6}$, Figure S1), but NOAA satellite-derived wind speeds were on average ~18% larger than WHOTS observations. Estimated k_w for cruises with both data products available also showed a strong correlation ($r^2 = 0.87$, $p < 10^{-6}$), with NCP_{0-mld} calculated using NOAA satellite-derived wind speeds being on average 22% larger than when using WHOTS data. Therefore, we applied a model II linear regression fit to correct NOAA-derived gas transfer velocities (Figure S1D) before calculating NCP_{0-mld} .

To account for wind speed variability prior to the measurements and calculate k_w , we used a 30-day weighted-averaging technique following Reuer et al. (2007) with the

modifications proposed by Teeter et al. (2018). In principle, equation (1) assumes that NCP_{0-mld} and air-sea gas exchange are at steady state. However, a recent analysis by Teeter et al. (2018) has demonstrated that independent of whether the assumption of steady state condition is valid or not, equation (1) approximates the exponentially weighted NCP_{0-mld} over the residence time of O_2 in the mixed water prior to the measurement. Residence times during our time series (estimated as the mixed layer depth divided by the gas transfer velocity for O_2) ranged between 5 and 30 days, with a mean value of 13 ± 6 days (\pm SD).

Another assumption of equation (1) is that the contributions of vertical and horizontal mixing to the O_2/Ar mass balance are negligible. The assumption of negligible horizontal mixing is supported by weak horizontal gradients of O_2 and Ar , which are the result of relatively fast air-sea gas exchange (Emerson et al., 1995, 1997). However, the contribution of vertical mixing, either through diapycnal mixing or entrainment, is not always negligible (see below).

2.4. GOP and R from a 24-hour cycle in O_2/Ar

Variations in O_2/Ar over a 24-hour cycle were used to estimate in situ rates of GOP and R. First, for each cruise, we determined a 24-hour time-series of biological O_2 concentration, $[O_2]_{bio}$, from O_2/Ar ratios:

$$[O_2]_{bio} = \frac{(O_2/Ar)_{meas}}{(O_2/Ar)_{eq}} [O_2]_{eq} \quad (3)$$

For each diel cycle, $[O_2]_{bio}$ was corrected for diffusive gas exchange since the first measurement:

$$[O_2]_{bio}^c(t) = [O_2]_{bio}(t) + \frac{1}{Z_{ML}} \int_{t_0}^t F_{bioO_2} dt \quad (4)$$

where t is time, t_0 is the time of the first measurement in the time-series, Z_{ML} is the depth of the mixed layer, and F_{bioO_2} is the air-sea diffusive gas exchange of $[O_2]_{bio}$, calculated as in equation (1) but using the instantaneous k_{O_2} instead of k_w . F_{bioO_2} is positive when the direction of exchange is from the ocean to the atmosphere.

The contributions of GOP and R to the diel variability in $[O_2]_{bio}^c$ were estimated following Barone et al. (2019b) by assuming that R is constant throughout the day and that

photosynthesis is linearly proportional to light intensity, which is assumed to vary as a simple function of solar elevation in cloud free conditions. The estimates of GOP and R were obtained using a linear least squares approach. Rate uncertainties were calculated by bootstrapping the residuals between $[O_2]_{bio}^C$ and the fitted model (Barone, et al., 2019b).

2.5. NCP below the mixed layer

The O_2 /Ar method estimates NCP in the mixed layer, which at Station ALOHA is always shallower than the euphotic zone. Therefore, to estimate NCP in the entire euphotic zone, we calculated NCP in the lower euphotic zone ($NCP_{mld-150m}$) by performing an O_2 mass balance using CTD O_2 profiles collected during consecutive HOT cruises. Considering the low temporal resolution of the data (near-monthly), for this analysis we used the HOT program time-series to expand our study period and then binned the results by month. We define the lower euphotic zone as the layer between the mixed layer depth and 150 m. This depth is very close to the mean compensation depth at Station ALOHA (155m, Laws et al., 2014) and matches the depth where gravitational particle C export is routinely measured by the HOT program. For each HOT cruise, we binned CTD dissolved O_2 profiles on potential density (to remove the effect of internal tides in the vertical displacements of isopycnals), and took the median O_2 profile. The CTD O_2 sensor is calibrated on each cruise against Winkler measurements (a description of sensor calibration can be found at http://www.soest.hawaii.edu/HOT_WOCE/oxyhist/3.html). The history of O_2 CTD sensors used since the beginning of the HOT program can be found at http://www.soest.hawaii.edu/HOT_WOCE/oxyhist/2.html. We chose to conduct our analysis between January 1996 and January 2019, after revised procedures to check for possible sensor problems were implemented in late 1995. We excluded HOT cruises 142 through 147 (November 2002 to April 2003) due to problems with the Winkler analyses (http://www.soest.hawaii.edu/HOT_WOCE/oxyhist/samp5.html). This approach assumes that $NCP_{mld-150m}$ have not significantly changed during this period. The mean absolute difference between matching CTD O_2 and Winkler O_2 measurements (\pm SD) in the upper 150 m for all cruises is 1.0 ± 1.3 mmol O_2 m^{-3} , or $< 0.5\%$ of dissolved O_2 .

$NCP_{mld-150m}$ between 2 consecutive cruises (with a period of time between them no longer than 60 days) was estimated as:

$$NCP_{mld-150m}(t) = Z_L \frac{[O_2]_{mld-150m}(t_2) - [O_2]_{mld-150m}(t_1)}{(t_2 - t_1)} \quad (5)$$

where t_1 and t_2 are the times of the two HOT cruises, t is the time between cruises, $[O_2]_{mld-150m}$ is the mean O_2 concentration (either at t_1 or t_2) in the layer between the base of the mixed layer at t_2 and 150 m, and Z_L is the thickness of the layer between the base of the mixed layer at t_2 and 150 m. These estimates do not account for fluxes of O_2 at the two boundaries: the base of the mixed layer and 150 m. In most cases, vertical mixing acts to decrease O_2 in the lower euphotic zone, therefore, $NCP_{mld-150m}$ should be considered as a conservative estimate. Conversely, our estimate of O_2 /Ar-derived NCP_{0-mld} will typically be an upper bound estimate since the vertical flux from below the mixed layer generally acts to increase O_2 in the mixed layer. That is, in some cases, NCP derived from mixed layer O_2 /Ar measurements includes a contribution from below the mixed layer. However, when we add NCP_{0-mld} and $NCP_{mld-150m}$, the contribution of O_2 mixing at the base of the mixed layer cancels out so that estimates of NCP for the entire euphotic zone are not affected by this uncertainty.

Since vertical diapycnal O_2 mixing can affect our NCP estimates, we assessed the potential uncertainty due to these fluxes by calculating the vertical O_2 gradients at the 150 m horizon and at the base of the mixed layer. The vertical gradients in O_2 were determined for each cruise from the median vertical profile in dissolved O_2 , binned on potential density to remove the effect of internal tides in vertical displacements of isopycnals (Haskell et al., 2016). The gradients at the base of the mixed layer and at 150 m were calculated as the slope of a linear regression between O_2 concentration and depth over a 10 m section, with the first point being at 150 m or at the base of the mixed layer, respectively.

2.6. Estimates of entrainment

To get an idea of to the extent to which entrainment might bias O_2 /Ar-derived NCP_{0-mld} we estimated the entrainment flux (E , $mmol\ O_2\ m^{-2}\ d^{-1}$) between HOT cruises occurring during October and December, when the seasonal deepening of the mixed layer generally occurs. To do this, we assume that NCP_{0-mld} in a cruise is affected by E when the mixed layer in the previous cruise was shallower, and E is estimated assuming that the rate of mixed layer deepening is constant between both cruises, so that:

$$E(t_2) = \frac{Z(t_2) - Z(t_1)}{t_2 - t_1} \times ([O_2]_{bio}(t_2) - [O_2]_E(t_1)) \quad (6)$$

where t_1 and t_2 are the times of the two HOT cruises, $[O_2]_{bio}$ is the concentration of biological O_2 in the mixed layer (as calculated from equation (3)), and $[O_2]_E$ is the mean O_2 concentration in the layer between the mixed layer depth (Z) at t_2 and t_1 . We avoid calculating E at other times of the year when the monthly climatology do not show a deepening of the mixed layer to avoid changes in mixed layer that might be caused by spatial variability or by episodic storm events (in these cases although there might be E , we cannot assume a constant rate of mixed layer deepening in between cruises).

2.7. Satellite-derived sea surface height anomalies

We obtained satellite measurements of sea surface height from the Copernicus Marine and Environment Monitoring Service (<http://marine.copernicus.eu>). We used the delayed time sea level anomaly (SLA) data product, which is obtained by merging the observations from all available satellites. SLA is defined as the signed difference (in cm) of sea surface height above the geoid with respect to its average during the 20 years reference period between 1993 and 2012. Corrected SLA, SLA_{corr} , was computed by interpolating SLA horizontally to estimate its value at Station ALOHA, and by removing the interannual trend and seasonal cycle (Barone et al., 2019a).

3. Results

3.1. Temporal variability in $\Delta O_2/Ar$

Measured O_2/Ar ratios in the mixed layer at Station ALOHA exceeded those expected at atmospheric equilibrium in most occasions, resulting in mostly positive $\Delta O_2/Ar$ values (Figure 1). Mean $\Delta O_2/Ar$ for each cruise varied between -0.09 and 1.67%, with a mean value for the time-series of 0.65 ± 0.41 % (\pm SD). $\Delta O_2/Ar$ values showed clear variations over a 24-hour cycle as well as seasonally. Over 24-hour cycles, minimum $\Delta O_2/Ar$ values typically occurred near sunrise and maximum values near sunset (Figure 2). This pattern is the result of biological activity, with the daytime increase in $\Delta O_2/Ar$ being a result of net primary production and the nighttime decrease resulting from community respiration (Ferrón et al., 2015). The amplitude of mixed layer $\Delta O_2/Ar$ variations over a 24-hour cycle ranged from 0.12 to 1.31%, with a mean

value of 0.39 ± 0.23 (\pm SD) %. Over an annual cycle, $\Delta O_2/Ar$ showed higher values in summer and fall, and lower values in winter and spring.

3.2. Mixed layer GOP and R from O_2/Ar variations over a 24-hour cycle

We obtained estimates of GOP and R from diel changes in O_2/Ar in 48 cruises (Figure 3A). In ~85% of occasions, the correlation between measured biological O_2 values and the theoretical sinusoidal curve used to estimate metabolic rates was significant ($p < 0.05$). The median r^2 for the fits was 0.82. In ~15% of occasions we obtained negative values for R, implying nighttime increases in O_2 relative to Ar, but all GOP values were positive. These negative rates were independent of the season. Mean values were obtained using a weighting approach based on the uncertainties in the rates (Barone et al., 2019b). The weighted mean GOP and R for the entire dataset were similar: 0.9 ± 0.5 and 0.8 ± 0.6 mmol O_2 m⁻³ d⁻¹ (weighted mean \pm weighted SD), respectively (Table 1). To avoid biases in our calculations, we included rates from poor fits (those with a $p > 0.05$) as well as negative rates that biologically would not make sense (Barone et al., 2019b). Excluding negative rates and poor fits would result in mean values that are ~9% and 15% larger for GOP and R, respectively (Table 1). The fit uncertainties for GOP and R individual rate estimates, computed as the SD obtained from bootstrapping the residuals, averaged 0.24 and 0.28 mmol O_2 m⁻³ d⁻¹, respectively. Given these fit uncertainties, the difference between diel GOP and R, or NCP estimated from diel O_2/Ar variations, is not significantly different from zero. The mean fit variance accounted for ~40% and 37% of the GOP and R weighted variance measured for all cruises, respectively. GOP and R were significantly correlated (Figure 4, $r^2 = 0.77$), indicating a coupling between the production and consumption of O_2 in the upper ocean. This correlation was not a bias due to the covariance of the two estimates from the least squares method (Figure S2). There was larger variability in R than GOP (Figure S2). GOP and R showed no clear seasonal trend (Figures 5A and B).

3.3. Net community production in the mixed layer

NCP_{0-mld} estimated for each cruise, which is the mean over a diel cycle, varied by more than an order of magnitude, from -0.7 to 17.6 mmol O_2 m⁻² d⁻¹ (mean \pm SD: 5.7 ± 3.8 mmol O_2 m⁻² d⁻¹) (Figure 3B). NCP_{0-mld} was positive in all but 3 cruises, indicating generally net autotrophic conditions. Diel GOP and NCP_{0-mld} were not significantly correlated ($p > 0.05$), but

NCP_{0-mld} showed a significant positive correlation with mean ¹⁴C-PP within the mixed layer ($r^2 = 0.36$, $p = 0.00002$). Volumetric NCP_{0-mld} rates (vNCP_{0-mld}), calculated by dividing NCP_{0-mld} by the mixed layer depth, ranged from -0.01 to 0.50 mmol O₂ m⁻³ d⁻¹ (mean \pm SD: 0.12 \pm 0.10 mmol O₂ m⁻³ d⁻¹). Both NCP_{0-mld} and vNCP_{0-mld} values showed a clear seasonal pattern, with higher values between May and August and lower values in the winter (Figures 5C and D). Diel changes in Δ O₂/Ar introduced on average ~23% variability (calculated for each diel cycle as the absolute coefficient of variation) in estimated NCP_{0-mld}. In comparison, the variability in areal NCP_{0-mld} for the entire time-series was ~66 %.

3.4. Net community production below the mixed layer

Month to month estimates of NCP_{mld-150m} based on HOT program observations (January 1996 to January 2019) varied widely, from -50.9 to 50.0 mmol O₂ m⁻² d⁻¹ (Figure 6B). However, the range of monthly mean values was much narrower, from -5.8 mmol O₂ m⁻² d⁻¹ in October to 7.2 mmol O₂ m⁻² d⁻¹ in April, averaging 0.6 \pm 4.5 mmol O₂ m⁻² d⁻¹. In comparison, the monthly mean NCP_{0-mld} ranged from 1.4 to 10.5 mmol O₂ m⁻² d⁻¹. The uncertainty associated with NCP_{mld-150m} is large, partly because our method is not Lagrangian and we could be interpreting horizontal variability as temporal changes. However, we assume that the horizontal variability in O₂ did not preferentially increase or decrease the estimate of NCP_{mld-150m} because from one month to the next it was equally likely to sample waters with higher or lower baseline O₂ inventory. For this reason, the effect of horizontal variability in NCP_{mld-150m} estimates would cancel out by averaging all rates over monthly intervals. Another factor affecting the accuracy of our NCP_{mld-150m} estimates is turbulent mixing, which causes vertical O₂ fluxes into and out of the lower euphotic zone. These fluxes take place both at the top and the bottom of the lower euphotic zone layer and they can be estimated as the product of the vertical O₂ gradient (mmol O₂ m⁻⁴) and the vertical diffusion coefficient (K_z , m² s⁻¹) at the boundary of the layer. Based on the sign of the O₂ gradient, vertical fluxes at 150 m resulted in a loss of O₂ from the layer in > 90% of the cases, causing an underestimation of NCP_{mld-150m}. Monthly mean O₂ gradients at 150 m ranged between -0.28 to -0.05 mmol O₂ m⁻⁴ (Figure 6C). Assuming a vertical diffusivity (K_z) of 10⁻⁵ m² s⁻¹ (Ledwell et al., 1993) these O₂ fluxes would increase NCP_{mld-150m} estimates by between 0.04 and 0.24 mmol O₂ m⁻² d⁻¹ (mean \pm SD: 0.12 \pm 0.05 mmol O₂ m⁻² d⁻¹). At the base of the mixed layer the monthly mean O₂ gradients showed a more pronounced seasonal variability (Figure

6C), ranging from -0.12 to 0.85 mmol O₂ m⁻⁴. Positive values, which occurred in 87% of occasions, imply an export of O₂ from the lower euphotic zone into the mixed layer, and as such result in an underestimation of NCP_{mld-150m} and an overestimation of NCP_{0-mld}. At the base of the mixed layer K_z is expected to be larger than below (Sun et al., 2013). In previous studies at Station ALOHA, K_z at the base of the mixed layer has been assumed to be between 0.1×10^{-4} and 1×10^{-4} m² s⁻¹ (Hamme & Emerson, 2006). Quay & Stutsman (2003) inferred that K_z at the base of the mixed layer needed to be roughly 0.5×10^{-4} m² s⁻¹ on an annual basis, to balance their diagnostic C balance model. In contrast, (Keeling et al., 2004) estimated K_z based on density gradients showing values of $\sim 0.1 \times 10^{-4}$ m² in summer and fall when stratification is strong, and of $\sim 0.4 \times 10^{-4}$ m² s⁻¹ in the winter. Here we assume a K_z of 0.5×10^{-4} m² s⁻¹ to estimate the monthly mean O₂ fluxes at the base of the mixed layer, ranging between -0.5 and 3.7 mmol O₂ m⁻² d⁻¹ (mean \pm SD: 1.3 ± 1.4 mmol O₂ m⁻² d⁻¹). The sensitivity of diapycnal O₂ fluxes at the base of the mixed layer to changes in K_z and vertical O₂ gradients is shown in Figure 7. Note that the magnitude of this flux, while uncertain, does not matter when adding up O₂/Ar-derived NCP_{0-mld} and NCP_{mld-150m}, as the fraction of NCP that escapes one layer is taken into account when estimating NCP in the next layer.

4. Discussion

4.1. Comparison of diel GOP and R with previous reported rate estimates

One of the advantages of assessing metabolism through time-resolved diel in situ sampling is that this approach provides a way to estimate metabolic rates without requiring incubations. Previous studies at Station ALOHA have reported differences in GOP rates measured using in vitro and in situ methods, with the latter generally resulting in larger values of up to $\sim 70\%$ (Juranek & Quay, 2005; Quay et al., 2010). However, the weighted-average rates obtained in this study fall well within the range of previously reported incubation-based measurements at Station ALOHA, although the range of all values is larger (Table 1, Figure 3A). Williams et al. (2004) used the light-dark bottle O₂ technique during a 1-year period at Station ALOHA. They reported GOP values in the upper 50m ranging between 0.3 and 1.3 mmol O₂ m⁻³ d⁻¹ (mean \pm SD: 0.8 ± 0.3 mmol O₂ m⁻³ d⁻¹), and R values from 0.3 to 1.5 mmol O₂ m⁻³ d⁻¹ (mean \pm SD: 0.9 ± 0.3 mmol O₂ m⁻³ d⁻¹). Published GOP measurements using the in vitro ¹⁸O-H₂O method (¹⁸O-GOP) in the upper 50 m at Station ALOHA range between 0.4 and 1.6 mmol O₂ m⁻³

d⁻¹ (Ferrón et al., 2016; Juranek & Quay, 2005; Quay et al., 2010). Between March 2006 and February 2008, ¹⁸O-GOP in the upper 50 m from a total of 21 cruises averaged 1.0 ± 0.3 (\pm SD) mmol O₂ m⁻³ d⁻¹ (Quay et al., 2010). Martínez-García & Karl (2015) used the in vivo INT method as a proxy to estimate R at Station ALOHA over the course of a year, with rates in the upper 100 m ranging from 0.3 to 1.5 mmol O₂ m⁻³ d⁻¹ (mean \pm standard error: 0.9 ± 0.1 mmol O₂ m⁻³ d⁻¹). In addition, the weighted-average rates obtained in this study are very similar to those obtained using the in situ diel O₂ approach from glider measurements (Barone et al., 2019b), which averaged 1.0 ± 0.7 mmol O₂ m⁻³ d⁻¹ for both GOP and R during four missions during spring and autumn. Nicholson et al. (2015) obtained higher mean GOP (1.8 ± 0.7 mmol O₂ m⁻³ d⁻¹) using a similar method during summer. Ferrón et al. (2015) also reported mean GOP and R values of 1.2 ± 0.1 and 1.0 ± 0.3 mmol O₂ m⁻³ d⁻¹ in a March cruise using the in situ O₂/Ar diel method. Relatively higher R rates were reported by Wilson et al. (2014) using continuous O₂ measurements in gliders near Station ALOHA, ranging between 2.4 and 4.6 mmol O₂ m⁻³ d⁻¹. It is more challenging to compare our rates with other non-incubation approaches, such as the triple O₂ method, as these rates are typically reported as areal estimates. However, rates of GOP derived using the in situ triple isotope O₂ method at Station ALOHA consistently exceeded those derived by the in vitro ¹⁸O-H₂O method by ~25-70% (Juranek & Quay, 2005; Quay et al., 2010), but our results agree well with the range of reported GOP using the in vitro ¹⁸O-H₂O method.

4.2. Validity of GOP and R derived from diel O₂/Ar measurements

In 85% of occasions, our observations showed a statistically significant fit to the theoretical diel O₂ curve ($p < 0.05$). In comparison, Nicholson et al. (2015) excluded ~30% of the data based on the lack of a significant fit between modeled values and measured O₂. Barone et al. (2019b) found that in ~30% of occasions either the fit was not statistically significant or the metabolic rates were negative and thus biologically improbable. These authors argued against excluding values from poor fits and negative rates as this could lead to a bias in the average rates, specifically it would likely result in an overestimation of the average rates by disproportionately excluding rates when the amplitude of O₂ is small due to lower rates. Instead they proposed to utilize a weighting average technique based on the uncertainty of the fits, which we also use here (Table 1). In this study, the percentage of poor fits ($p > 0.05$) and negative rates was also ~30%, however, in contrast to the results from Barone et al. (2019b) who found

negative values in either GOP or R rates, we only obtained negative R rates (all GOP estimates were positive). The reason for this is unknown. In any case, excluding poor fits and negative rates would result in weighted mean GOP and R rates that are only 11% and 16% higher, respectively, than when all values are included (Table 1).

An approach we can use to evaluate the validity of our in situ rates is to compare them to rates measured on HOT cruises using alternative methods, such as dawn to dusk ^{14}C assimilation rates. One consideration when comparing these values is that the sampling for ^{14}C -PP typically occurs 14 hours before the initial sampling for O_2/Ar (that covers a 24-hour period). The different sampling time not only means a different temporal coverage but also that the two estimates are from different water parcels due to the Eulerian sampling of a heterogeneous ocean. Despite this, we found a weak but significant positive correlation ($r^2 = 0.19$, $p=0.003$) between diel GOP and ^{14}C -PP for the mixed layer, indicating that both independent methods tracked similar trends in primary productivity. Rates of GOP were on average 1.7 ± 1.0 times larger than ^{14}C -PP ($\text{mol O}_2 \text{ mol C}^{-1}$). This difference is expected as, due to respiration of labeled organic C and re-fixation of respired $^{14}\text{CO}_2$ during the incubation, ^{14}C uptake in dawn to dusk incubations yields a value that is thought to approximate net primary production rather than GPP (Marra, 2002, 2009). In addition, the production of dissolved organic ^{14}C , if not measured, results in an underestimation of productivity by the ^{14}C method (Karl et al., 1998). A compilation of measurements collected by the Joint Global Ocean Flux Study (JGOFS) program from different marine environments showed a fairly constant ratio of ^{18}O -GOP and 24-hour ^{14}C -PP (Marra, 2002). The mean ratio from these observations was $2.7 \text{ mol O}_2 \text{ mol C}^{-1}$, which would be equivalent to $2.0 \text{ mol O}_2 \text{ mol C}^{-1}$ for ^{14}C incubations lasting 12 hours instead of 24 hours (Juranek & Quay, 2012; Marra, 2002). Nearly-monthly measurements over a 2-year period at Station ALOHA yielded a mean ^{18}O -GOP to ^{14}C -PP (12-hour) ratio of $1.9 \pm 0.5 \text{ mol O}_2 \text{ mol C}^{-1}$ (Quay et al., 2010), consistent with the JGOFS compilation (Marra, 2002). However, concurrent in situ $^{17}\Delta$ -GOP measurements exceeded ^{18}O -GOP by 25-60%, and yielded a mean $^{17}\Delta$ -GOP to ^{14}C -PP (12-hour) ratio of $2.5 \text{ mol O}_2 \text{ mol C}^{-1}$ (Quay et al., 2010). These authors suggested that the discrepancy between both methods could be due to an underestimation of productivity by the incubation approach, either due to missed stochastic productivity events (Karl, et al., 2003b) or, more likely, due to biases introduced in bottle incubations associated to the perturbation of the environmental conditions. However, the mean GOP to ^{14}C -PP (12-hour) for this study, 1.7 ± 1.0

mol O₂ mol C⁻¹, using in situ diel GOP estimates, is more in line with those obtained using the in vitro ¹⁸O method and lower than those derived from the in situ ¹⁷Δ method. Both the ¹⁸O and ¹⁷Δ methods provide a measurement of gross O₂ production from splitting water, regardless of whether the production of O₂ is linked to the fixation of C. As such, the ¹⁸O and ¹⁷Δ methods overestimate GOP to the extent that the Mehler reaction and photorespiration occur, typically by 15-20% (Bender et al., 1987; Laws et al., 2000). By multiplying the ¹⁸O-GOP and ¹⁷Δ-GOP estimates by 0.85 to correct for the Mehler reaction and photorespiration (Juranek & Quay, 2005), the mean GOP to ¹⁴C-PP reported by Quay et al. (2010) would be 1.6 and 2.1, respectively, and therefore, the ratio determined in this study from in situ diel changes in O₂/Ar would still be more similar to that derived by the incubation-based method. However, GOP measurements using the in vitro light-dark O₂ method over a one-year study at Station ALOHA yielded GOP to ¹⁴C-PP ratios of 1.2 to 1.5 mol O₂ mol C⁻¹ in the upper 50 m of the water column (Williams et al., 2004), ~12 to 29 % lower than the mean ratio derived from this study.

4.3. Diel variability in biological O₂

The mean diel cycle in biological O₂ at Station ALOHA shows that the net rates of O₂ production and consumption in the mixed layer are not constant throughout the day. During daytime, net O₂ production starts after 6:00 (~ local dawn), but the majority of O₂ production occurs on average between 9:00 and 15:00, after which the mixed layer becomes net heterotrophic until the next morning (Figure 2C). Similarly, during nighttime the mean rate of O₂ consumption is not constant, being lowest in the hours before dawn. A similar pattern was reported by Barone et al. (2019b) near Station ALOHA, and together with our observations support the idea that R might vary throughout the day due to changes in the availability of fresh organic matter produced by photosynthesis (e.g. Sadro et al., 2011; Viviani & Church, 2017; Weger et al., 1989). The assumption of constant R throughout the day in our model could therefore introduce uncertainty in our estimates.

4.4. Seasonal variability in GOP and R

The 30-year record at Station ALOHA show that the depth-integrated values of ¹⁴C-PP for the euphotic zone follow a seasonal trend, with higher rates in the summer and lower rates in the winter. The seasonal variability in ¹⁴C-PP is partly driven by variations in photosynthetically

available radiation (PAR) throughout the year (Karl & Church, 2017). In our time-series, mixed layer ^{14}C -PP also showed a seasonal pattern of higher values in the summer and lower values in the winter (Figure S3), with a ~2-fold change in mixed layer ^{14}C -PP throughout the year, and a coefficient of variation for the entire dataset of ~27%. In contrast, we did not observe a clear seasonal pattern for mixed layer diel GOP and R estimates (Figures 5A and B). The uncertainty of GOP and R estimates from diel O_2/Ar measurements was on average ~38% and ~48% of individual GOP and R, respectively, which may preclude detection of seasonal variability. Similarly, in situ $^{17}\Delta$ -GOP values did not show a clear seasonal pattern during a 2-year study at Station ALOHA, when concurrent in vitro ^{18}O -GOP showed a seasonal trend with summer values being approximately 30% higher than winter values (Quay et al., 2010). Additionally, previous studies have shown considerable short term variability in diel GOP and R estimates (Barone et al., 2019b; Ferrón et al., 2015), so the lack of seasonal variability could also be due to the fact that we are basing our estimates on a single 24-hour cycle for each cruise, which might not be representative of the season.

4.5. Influence of entrainment and vertical mixing on O_2/Ar -derived rates

At Station ALOHA, O_2 accumulates below the mixed layer as this layer shoals during the spring and until it deepens during the fall (Shulenberger & Reid, 1981; Figure 6A). Therefore, entrainment of high O_2/Ar water from below during fall months (between September and December) could violate the steady state assumption and lead to an overestimation of $\text{NCP}_{0-\text{mld}}$ (Nicholson et al., 2012). Estimates of diel GOP and R are not affected by entrainment, unless the entrainment of water occurred during the time of the measurements. $\text{NCP}_{0-\text{mld}}$ estimates are only affected by entrainment that occurred within the residence time of the O_2 prior to O_2/Ar measurements. We did not attempt to correct $\text{NCP}_{0-\text{mld}}$ values for entrainment because the mixed layer depth history prior to the measurements was unknown. However, we estimated mean entrainment fluxes between HOT cruises occurring during October and December, when the seasonal deepening of the mixed layer generally occurs, to get an idea of the extent to which these fluxes might bias mixed layer O_2/Ar -derived $\text{NCP}_{0-\text{mld}}$. Estimates of entrainment averaged $-3.8 \pm 1.6 \text{ mmol O}_2 \text{ m}^{-2} \text{ d}^{-1}$ in October and November, and $-2.3 \pm 1.7 \text{ mmol O}_2 \text{ m}^{-2} \text{ d}^{-1}$ in December (Figure 8A). This means that entrainment could potentially account for ~55% of monthly O_2/Ar -derived $\text{NCP}_{0-\text{mld}}$ in October and November, and ~100% in December, reducing

annual $\text{NCP}_{0\text{-mld}}$ by ~15%. In addition to entrainment events, another process that could bias O_2/Ar -derived rates is diapycnal mixing across the base of the mixed layer. During the summer and fall months, due to the presence of the seasonal O_2 subsurface maximum (Shulenberger & Reid, 1981; Figure 6A), the gradients at the base of the mixed layer are elevated (Figure 6C). However, these months also coincide with the presence of stronger density gradients that might result in lower K_z at the base of the mixed layer (Keeling et al., 2004). Assuming that K_z at the base of the mixed layer has an annual value of $0.5 \times 10^{-4} \text{ m}^2 \text{ s}^{-1}$, monthly mean vertical O_2 diffusive fluxes indicate that NCP formed below the mixed layer might contribute up to ~70 % to $\text{NCP}_{0\text{-mld}}$ estimates in September (Figure 8A). In January and February, the O_2 gradients at the base of the mixed layer are negative, indicating that $\text{NCP}_{0\text{-mld}}$ during those months might be underestimated by ~30%. On an annual basis, accounting for vertical diffusive fluxes (assuming a K_z of $0.5 \times 10^{-4} \text{ m}^2 \text{ s}^{-1}$ at the base of the mixed layer) would reduce estimated annual $\text{NCP}_{0\text{-mld}}$ by ~23%. However, the magnitude of vertical O_2 diffusive fluxes scales linearly with K_z (Figure 7), which is poorly constrained due to the scarcity of its measurements. If during the summer and fall months K_z was $0.1 \times 10^{-4} \text{ m}^2 \text{ s}^{-1}$ (Keeling et al., 2004), monthly mean vertical O_2 diffusive fluxes would range between -0.5 and 0.9 $\text{mmol O}_2 \text{ m}^{-2} \text{ d}^{-1}$ (mean \pm SD: $0.3 \pm 0.4 \text{ mmol O}_2 \text{ m}^{-2} \text{ d}^{-1}$), and the resulting annual $\text{NCP}_{0\text{-mld}}$ when accounting for these fluxes would be reduced by ~5%.

To estimate the effects of vertical diapycnal fluxes in diel GOP and R we divided mean monthly vertical O_2 fluxes by the mean depth of the mixed layer. Resulting volumetric O_2 fluxes estimated assuming an annual K_z of $0.5 \times 10^{-4} \text{ m}^2 \text{ s}^{-1}$ are relatively small compared to GOP and R rates, ranging from -0.01 to 0.06 $\text{mmol O}_2 \text{ m}^{-3} \text{ d}^{-1}$ and contributing on average ~3% to the monthly rates.

4.6. Net community production

4.6.1. Seasonal variability $\text{NCP}_{0\text{-mld}}$

Monthly means of O_2/Ar -derived $\text{NCP}_{0\text{-mld}}$ show a clear seasonal pattern, with low values between December and February ($1.8 \pm 0.4 \text{ mmol O}_2 \text{ m}^{-2} \text{ d}^{-1}$), a progressive increase between February and May, and high values between May and August ($8.7 \pm 1.6 \text{ mmol O}_2 \text{ m}^{-2} \text{ d}^{-1}$). September shows an abrupt decrease in mean $\text{NCP}_{0\text{-mld}}$ of ~60 % compared to August, followed by a ~2-fold increase in October, to then progressively decrease between October and December (Figure 8A). The general seasonal $\text{NCP}_{0\text{-mld}}$ pattern in this study, with lower $\text{NCP}_{0\text{-mld}}$ values in

winter and higher values in summer and fall is consistent with the overall seasonality of ^{14}C -PP (Karl & Church, 2017), ^{18}O -GOP (Quay et al., 2010), and that of particulate matter standing stocks (Hebel & Karl, 2001). The abrupt decrease in $\text{NCP}_{0\text{-mld}}$ during September might be related to the recurrent sudden increase of deep sea particle fluxes in August that was reported by Karl et al. (2012). This enigmatic phenomenon is thought to be a consequence of the summertime increase of symbiotic N_2 -fixing cyanobacteria in association with diatoms. The environmental cue that initiates particle aggregation and subsequent rapid export to the seafloor is unknown, but it has been hypothesized to be changes in day length (Karl et al., 2012). The monthly seasonal climatology of upper ^{14}C -PP rates (0-45m), as well as particulate C export fluxes at 150 m, also show a decrease in September of ~20-30% compared to August (Figures S4B and S5A). However, $\text{NCP}_{0\text{-mld}}$ increases again in October before decreasing in the winter. This rapid increase in $\text{NCP}_{0\text{-mld}}$ in October could partly be due to an overestimation of $\text{NCP}_{0\text{-mld}}$ due to the entrainment of O_2/Ar rich water from below at the onset of the mixed layer seasonal deepening and/or to diapycnal fluxes (Figure 8A).

4.6.2. Influence of mesoscale processes on $\text{NCP}_{0\text{-mld}}$

At Station ALOHA mesoscale physical variability, measured as changes in sea surface height, has been linked to changes in the upper column standing stocks of N and P, with concentrations of total dissolved N and P significantly increasing with SLA (Barone et al., 2019a; Church et al., 2009). These changes are not directly coupled to the displacement of layers of water but presumably are the result of a biological ecosystem response to mesoscale dynamics. In addition, SLA was found to be inversely correlated to the eukaryotic biomass at the DCM, as a consequence of the increase in the vertical supply of nutrients associated with the uplifting of isopycnal surfaces and subsequent enhancement of diapycnal fluxes (Barone et al., 2019a). Because rates of ^{14}C -PP at the DCM were independent of variations in SLA, the authors hypothesized that the increase in biomass was a result of an increase in NCP but not GOP. Similarly, Nicholson et al. (2008) also demonstrated the effect of mesoscale processes in net O_2 rates below the mixed layer, which were elevated during periods of isopycnal shoaling. In addition to physical processes, N_2 fixation may supply up to half of the N needed to support new production (Böttjer et al., 2017; Dore et al., 2002). Variations in N_2 fixation rates and the dominant diazotrophic community have also been linked to mesoscale physical processes

(Böttjer et al., 2017; Church et al., 2009). Specifically, episodically high rates of N_2 fixation are typically associated with the proliferation of larger filamentous diazotrophs that occur during periods of high SLA, warm temperatures, and high light fluxes (Church et al., 2009). Because of the potential of mesoscale physical forcing affecting NCP, we tested whether changes in SLA have an effect on rates of NCP_{0-mld} . NCP_{0-mld} in this study was not significantly correlated with SLA ($p > 0.05$), but larger NCP_{0-mld} rates were observed when SLA values were extreme (either larger than 9 cm or lower than -9 cm), compared to intermediate values (one-way ANOVA, $p < 0.05$) (Figure S6). However, when the effect of the seasonal signal was removed by subtracting the monthly mean from each point of the time series, the relationship was no longer significant. One would expect that the influence of mesoscale processes on NCP would be more noticeable in the lower portion of the euphotic zone (Barone et al., 2019a). Unfortunately, our estimates of $NCP_{mld-150m}$ are climatological monthly averages and thus, our analysis does not allow us to investigate this relationship.

4.6.3. Incorporating NCP below the mixed layer

The mixed layer depth monthly climatology at Station ALOHA, calculated as described in section 2.2, oscillates between ~40 m in the summer and ~85 m in the winter (mean \pm SD: 60 ± 16 m). Therefore, by estimating NCP in the mixed layer we in principle neglect the deeper portion of the euphotic zone where an important fraction of new production occurs (Letelier et al., 1996, 2004). A few studies have estimated NCP in the lower portion of the euphotic zone beneath the mixed layer near or at Station ALOHA using an O_2 mass balance approach. Hamme & Emerson (2006) estimated annual NCP in this region to be between 0 and $0.9 \text{ mol } O_2 \text{ m}^{-2} \text{ yr}^{-1}$, depending on whether K_z was assumed to be $0.1 \times 10^{-4} \text{ m}^2 \text{ s}^{-1}$ or $1 \times 10^{-4} \text{ m}^2 \text{ s}^{-1}$. Using O_2 measurements collected from gliders, Nicholson et al. (2008) estimated NCP in the lower euphotic zone to be between $0.9 \text{ mol } O_2 \text{ m}^{-2} \text{ yr}^{-1}$ and $1.5 \text{ mol } O_2 \text{ m}^{-2} \text{ yr}^{-1}$, depending on whether diapycnal mixing was assumed negligible or $1 \times 10^{-4} \text{ m}^2 \text{ s}^{-1}$. Similarly, Riser and Johnson (2008) used O_2 measurements from profiling floats to estimate NCP as a function of depth, showing that ~25% of annual NCP takes place below the mixed layer depth ($\sim 0.6 \text{ mol } O_2 \text{ m}^{-2} \text{ yr}^{-1}$). Our estimates of $NCP_{mld-150m}$ are considered a lower bound because the diapycnal O_2 fluxes across the top and bottom layer boundaries are not taken into consideration (Figure 8B), resulting in an annual $NCP_{mld-150m}$ of 0.21 ± 0.13 (\pm SD) $\text{mol } O_2 \text{ m}^{-2} \text{ yr}^{-1}$, much lower than the estimates

reported by Nicholson et al. (2008) and Riser and Johnson (2008), but within the range reported by Hamme & Emerson (2006). However, adding diapycnal O_2 fluxes at the base of the mixed layer (assuming $K_z = 0.5 \times 10^{-4} \text{ m}^2 \text{ s}^{-1}$) and at the 150 m reference depth (assuming $K_z = 0.1 \times 10^{-4} \text{ m}^2 \text{ s}^{-1}$) would increase annual $NCP_{\text{mld-150m}}$ by $0.48 \text{ mol } O_2 \text{ m}^{-2} \text{ yr}^{-1}$ and $0.04 \text{ mol } O_2 \text{ m}^{-2} \text{ yr}^{-1}$, respectively. The resulting annual $NCP_{\text{mld-150m}}$ of $0.65 \text{ mol } O_2 \text{ m}^{-2} \text{ yr}^{-1}$ is more in line with previously published estimates (Hamme & Emerson, 2006; Nicholson et al., 2008; Riser & Johnson, 2008). During the months when the mixed layer shoals and the seasonal subsurface O_2 accumulation occurs, O_2/Ar -derived $NCP_{0-\text{mld}}$ estimates incorporate the O_2 diapycnal fluxes across the base of the mixed layer, that is, a considerable portion of $NCP_{0-\text{mld}}$ might have taken place below it (Figure 8A). By adding monthly $NCP_{\text{mld-150m}}$ to O_2/Ar -derived $NCP_{0-\text{mld}}$ we eliminate the need to correct for the diapycnal fluxes at the base of the mixed layer, and the correction for diapycnal fluxes at 150 m is small. This results in total monthly NCP for the euphotic zone ($NCP_{0-150\text{m}}$) ranging between -0.7 and $14.5 \text{ mmol } O_2 \text{ m}^{-2} \text{ d}^{-1}$ (Figure 8C). Because a considerable portion of $NCP_{0-\text{mld}}$ might already incorporate a fraction of lower euphotic NCP, we estimate that annual $NCP_{0-150\text{m}}$ is only $\sim 10\%$ larger than annual $NCP_{0-\text{mld}}$ derived from mixed layer O_2/Ar measurements alone (Table 2).

The monthly climatology in NCP estimates in the lower euphotic zone shows a very different pattern than the mixed layer (Figure 8B). $NCP_{\text{mld-150m}}$ is positive during the months where the mixed layer is shoaling, January through May, to then become negative for the rest of the year, with the exception of July and September. The larger $NCP_{\text{mld-150m}}$ at the beginning of the year is consistent with the observations by Letelier et al. (2004), who found that the deepening of isolumes in early spring resulted in the availability of nitrate (previously unavailable due to light limitation) and the consequent increase of phytoplankton biomass at the deep chlorophyll maximum layer, which the authors compared to a spring bloom event.

Similarly, primary production at Station ALOHA, measured as ^{14}C assimilation, shows distinct seasonal patterns at the surface (0-45 m) and at the lower euphotic zone (75-125 m) (Figure S4, Winn et al., 1995). Whereas seasonal cycles of primary production in the lower euphotic zone are mostly driven by changes in solar irradiance (Letelier et al., 2004), increasing between December and June and decreasing between June and December, primary production in the upper part of the water column remains high until late summer (Figure S4). As mentioned

before, the higher rates of surface primary production and $\text{NCP}_{0\text{-mld}}$ in late summer are thought to be driven by increasing rates of N_2 fixation that relieves the system from N limitation. So while O_2/Ar -derived $\text{NCP}_{0\text{-mld}}$ tracks the seasonality of ^{14}C -PP, seasonal variability in $\text{NCP}_{\text{mld-150m}}$ does not seem to be solely driven by changes in primary production (Figure 8B). When taken together, our monthly estimates of NCP down to 150 m (Figure 8C) show a different seasonality than $\text{NCP}_{0\text{-mld}}$. Monthly means of $\text{NCP}_{0\text{-150m}}$ experience a gradual increase from January to May, with a significant drop in total NCP in June. Between June and September monthly $\text{NCP}_{0\text{-150m}}$ is relatively constant, averaging $6.9 \pm 1.0 \text{ mmol O}_2 \text{ m}^{-2} \text{ d}^{-1}$, to then show another drop (~ 3 -fold) in October, and continue to decrease until December, when our estimates indicate that the euphotic zone is temporarily net heterotrophic. Therefore, the net production of O_2 in the euphotic zone shows an intriguing seasonal pattern that is uncoupled from monthly depth-integrated ^{14}C assimilation (0-125 m) and C export by sinking particles at 150 m (Figures S4 and S5). $\text{NCP}_{0\text{-150m}}$ shows a strikingly large dynamic range with monthly values varying by over an order of magnitude. In comparison, ^{14}C -PP and gravitational C export at 150 m vary monthly by ~ 2 -2.5 fold. Interestingly, our estimates imply that the euphotic zone becomes net heterotrophic in December, despite the measurable export of sinking particles during that month. It is also possible that net heterotrophy is reached earlier in the year (in October or November) if our estimates of total NCP are overestimated due to the effect of entrainment. This decoupling between particle export and $\text{NCP}_{0\text{-150m}}$ could be due to the consumption of organic matter accumulated during previous months (Hebel & Karl, 2001).

4.6.4. Annual NCP and interannual variability

At steady state, net community production integrated over an annual cycle equals the export of biologically-produced organic C from the euphotic zone, also known as the biological C pump. We estimate annual NCP for the euphotic zone for our study period to be $2.4 \pm 0.5 \text{ mol O}_2 \text{ m}^{-2} \text{ yr}^{-1}$ (Table 2) or $1.7 \pm 0.4 \text{ mol C m}^{-2} \text{ yr}^{-1}$, assuming a photosynthetic quotient of 1.4 (Laws, 1991). Our estimate is well within the range of previously reported values at or near Station ALOHA, ranging between 1.0 and $4.2 \text{ mol C m}^{-2} \text{ yr}^{-1}$ (Table 3). At Station ALOHA, the mean particulate organic C flux by sinking particles between 1988 to 2013 determined using sediment traps is $0.8 \pm 0.3 \text{ mol C m}^{-2} \text{ yr}^{-1}$, and $0.9 \pm 0.2 \text{ mol C m}^{-2} \text{ yr}^{-1}$ for our study period. However, the gravitational settling of particles measured using sediment traps, which represent

the only core measurement of export production by the HOT program, may not be a good reflection of the biological C pump due to the potentially important contributions by other mechanisms to the export of sinking, suspended, and dissolved organic matter (Boyd et al., 2019). These other mechanisms include: (i) the physical subduction of particles (and dissolved organic matter) due to the seasonal shallowing of the mixed layer, large scale circulation, and mesoscale or subscale frontal circulation (Boyd et al., 2019 and references therein), (ii) the active transport by migrating zooplankton (Boyd et al., 2019; Hannides et al., 2009), and (iii) the diffusive flux of dissolved organic matter (Emerson, 2014). During our study period the gravitational settling of particles captured in sediment traps at 150 m accounted on average for 53% of NCP_{0-150m} (converted to C units assuming a photosynthetic quotient of 1.4) (Table 2). At Station ALOHA, the diurnal vertical migration of zooplankton was estimated to account on average for 19% of C export by sinking particles (Hannides et al., 2009), that is, approximately $\sim 0.17 \text{ mol C m}^{-2} \text{ yr}^{-1}$ for our study period (or $\sim 10\%$ of NCP_{0-150m}). The diffusive flux of dissolved organic C at 150 m can be estimated based on measurements collected by the HOT program and assuming a $K_z = 0.1 \times 10^{-4} \text{ m}^2 \text{ s}^{-1}$. Although measurements of dissolved organic C during the period of our study were not available, we estimated the mean diffusive flux during the period between 2002 and 2010 (prior years were not included due to the use of a different methodology). The estimated diffusive flux of dissolved organic matter at 150 m is $0.05 \pm 0.02 \text{ mol C m}^{-2} \text{ yr}^{-1}$, contributing by less than 3% to NCP_{0-150m} . Under the assumption that our estimate of net community production is a good proxy of C export production, alternative export mechanisms (Boyd et al., 2019) other than the passive sinking of particles as measured by sediment traps, the active transport by zooplankton, and the diffusive flux of dissolved organic C are needed to account for up to 35% of the biological C pump. Previous studies have suggested that particle flux measurements from shallow surface-tethered sediment traps might be biased, typically showing an under-collection of particles compared to the ^{234}Th disequilibrium method (Benitez-Nelson et al., 2001; Buesseler, 1991). Therefore, under-collection of particles by the sediment traps is also a plausible explanation for the discrepancy.

The mean mixed layer NCP_{0-mld}/GOP ratio for our study period was 0.11 ± 0.07 (Table 2), indicating that most of the O_2 produced in the mixed layer is consumed by respiratory processes. In comparison, Juranek & Quay (2005) reported mixed layer $NCP/^{17}\Delta\text{-GOP}$ values at Station ALOHA ranging from -0.13 in winter to 0.13 in summer, whereas Quay et al. (2010)

estimated $\text{NCP}/^{17}\Delta\text{-GOP}$ values of 0.12 ± 0.05 in winter and 0.22 ± 0.08 in summer. To evaluate export efficiency in the entire euphotic zone we look at the ratio of annual $\text{NCP}_{0-150\text{m}}$ to depth-integrated $^{14}\text{C-PP}$, as our estimates of diel GOP do not extend below the mixed layer depth. The mean $\text{NCP}_{0-150\text{m}}/^{14}\text{C-PP}$ of 0.10 ± 0.03 is also indicative of a system where primary production is mostly sustained by recycled nutrients. This ratio is smaller than that reported by Brix et al. (2006) for years 1988-2002 (0.22 ± 0.03). The reason for this discrepancy is a combination of a long-term increase in NPP at Station ALOHA (Kavanaugh et al., 2018) and our lower estimates of annual NCP.

Interannual variability of annual $\text{NCP}_{0-150\text{m}}$ in the first 4 years of the study period was low, with a coefficient of variation of $\sim 7\%$. However, when 2018 is included in the analysis the variability increases to $\sim 25\%$. This is because annual $\text{NCP}_{0-150\text{m}}$ in 2018 was anomalously low, 44% lower than the 2014-2018 mean value (Table 2). That year also coincided with the lowest depth-integrated $^{14}\text{C-PP}$ of our time series (Table 2). Annual $\text{NCP}_{0-150\text{m}}$ and NPP were significantly and positively correlated ($r^2 = 0.94$, $p = 0.006$), indicating that enhanced C export occurs during years with higher primary production. However, the $\text{NCP}_{0-150\text{m}}/^{14}\text{C-PP}$ ratio, or fraction of NPP that is exported from the euphotic zone, was also lower in 2018 compared to the other years, which would be suggestive of more efficient recycling (through grazing and/or heterotrophic respiration) during years of lower productivity. In contrast to the statistically significant correlation between annual $\text{NCP}_{0-150\text{m}}$ and NPP, particulate C export was not significantly correlated to annual NPP or $\text{NCP}_{0-150\text{m}}$ ($p > 0.05$). Although NPP and particulate C export might be temporally decoupled (Buesseler, 1998; Karl et al., 1996; Karl & Church, 2017), it is surprising that they do not track each other when integrated over a year. An analysis of more than 10 years of data at Station ALOHA found no significant correlation between annual NCP, NPP and particulate C flux (Brix et al., 2006). The authors attributed the high scatter obtained in the interannual analyses to biases introduced by under-sampling episodic events, which might affect annual means but would probably not affect long-term seasonal means. Due to the decoupling of particle export and primary production, it is conceivable that under-sampling might affect the integrated annual values of NCP, NPP and particulate C export differently. In addition, the extent of undersampling might differ for the different variables. During our study period, the deployment of the sediment traps or the ^{14}C primary production array had to be cancelled on a number of occasions due mostly to bad weather, affecting the annual coverage for

those measurements. Approximately 20% of cruises between 2014-2018 where we collected O_2/Ar data do not have concurrent sediment trap export flux measurements, and ~10% do not have ^{14}C -PP data. The coverage was particularly low in 2018, with only 5 and 6 cruises with sediment trap and ^{14}C -PP data for the entire year, and only 8 cruises with O_2/Ar measurements (there are typically 10 cruises per year).

5. Summary and conclusions

In the NPSG, mixed layer $\Delta O_2/Ar$ varies over a diel cycle due to the biological processes of photosynthesis and respiration, with values increasing during daytime and decreasing during nighttime. Estimates of in situ mixed layer GOP and R from $\Delta O_2/Ar$ variations over a 24-cycle, averaging 0.9 ± 0.5 and 0.8 ± 0.6 mmol O_2 m⁻³ d⁻¹ respectively, are in good agreement with previous rates estimated using both in vitro and in situ diel methods in the same environment, but lower than previous GOP estimates using the in situ triple isotope O_2 method. The mean rates of net biological O_2 change for this study indicate that R may not be constant throughout the day, an assumption in our model. Diel GOP and R co-varied, indicating a tight coupling between the production and consumption of O_2 in the mixed layer, but did not show a clear seasonal pattern. Increasing the time period used for our calculations could improve the accuracy of these estimates.

NCP in the NPSG showed pronounced seasonality, with a much larger dynamic range than other measures of production such as diel GOP, ^{14}C assimilation, and gravitational C export. During summer and fall, the diapycnal flux of O_2 across the mixed layer may be considerable and, therefore, a fraction of NCP derived from mixed layer O_2/Ar measurements may be formed below the mixed layer. Additionally, between October and December, when the mixed layer deepens, the entrainment of O_2/Ar -rich water could result in an overestimation of NCP_{0-150m}. Monthly means of NCP in the mixed layer and in the lower euphotic zone show very different patterns. The resulting seasonality of NCP for the euphotic zone shows a maximum in May and a minimum in December, when the system becomes temporarily net heterotrophic, despite observations of persistent vertical export through sinking particles. Such observations highlight the decoupling between the seasonal pattern of NCP_{0-150m} and the gravitational C export measured by sediment traps.

Our estimates indicate that annual NCP for the euphotic zone at Station ALOHA is 2.4 ± 0.5 mol O_2 m⁻² yr⁻¹, or 1.7 ± 0.4 mol C m⁻² yr⁻¹ if we assume a photosynthetic quotient of 1.4.

This value, within the range of previous estimates in the same environment, is about twice the export of C by sinking particles measured using sediment traps, suggesting that additional, largely unquantified mechanisms of C export might be important in this ecosystem.

Acknowledgments

We thank the dedicated efforts of the HOT team who facilitated this work and assisted with sample collection, as well as the captains and crew of R/V *Kilo Moana* and R/V *Kaimikai-O-Kanaloa* for safe and efficient field operations. Additionally, we thank Gerianne Terlouw, Macarena Burgos, and Andrés Salazar for helping with O₂/Ar analyses. The buoy wind data are available online at <http://uop.whoi.edu/projects/WHOTS/whotsdata.htm> and are from the WHOTS mooring, which is supported by the National Oceanic and Atmospheric Administration (NOAA) through the Cooperative Institute for Climate and Ocean Research (CICOR) under Grant No. NA17RJ1223 and NA090AR4320129 to the Woods Hole Oceanographic Institution, and by National Science Foundation (NSF) grants OCE-0327513, OCE-752606, and OCE-0926766 to the University of Hawaii for the Hawaii Ocean Time-series. Blended Sea Winds are distributed by NOAA-NCDC and are available at <https://www.ncdc.noaa.gov/data-access/marineocean-data/blended-global/blended-sea-winds>. Sea-level pressure from the NCEP/NCAR reanalysis is available at <https://www.esrl.noaa.gov/psd/data/gridded/data.ncep.reanalysis.surface.html>. Data from the HOT program are available at <https://hahana.soest.hawaii.edu/hot/hot-dogs/>. The rest of the data presented here are available at <https://doi.org/10.5281/zenodo.3936089> and will also be available at the Simons Collaborative Marine Atlas Project (<https://simonscmap.com/>). This research was supported by the 2015 Balzan Prize for Oceanography (awarded to D.M.K.), the Simons Foundation (Simons Collaboration on Ocean Processes and Ecology, award 329108 to D.M.K., A.E.W., and M.J.C.), the Gordon and Betty Moore Foundation (grant #3794 to D. M. K) and NSF through the Center of Microbial Oceanography: Research and Education (C-MORE, EF04-24599 to D. M. K) and the HOT program (OCE-0926766 and OCE-1260164 to M.J.C. and D.M.K., and OCE-1756517 to A.E.W. and D.M.K.).

References

Barone, B., Coenen, A. R., Beckett, S. J., McGillicuddy, D. J., Weitz, J. S., & Karl, D. M.

806 (2019a). The ecological and biogeochemical state of the north pacific subtropical gyre is
 807 linked to sea surface height. *Journal of Marine Research*, 77, 215–245.
 808 <https://doi.org/10.1357/002224019828474241>

809 Barone, B., Nicholson, D. P., Ferrón, S., Firing, E., & Karl, D. M. (2019b). The estimation of
 810 gross oxygen production and community respiration from autonomous time-series
 811 measurements in the oligotrophic ocean. *Limnology and Oceanography: Methods*, 17(12),
 812 650–664. <https://doi.org/10.1002/lom3.10340>

813 Bender, M., Grande, K., Johnson, K., Marra, J., Williams, P. J. le. B., Sieburth, J., et al. (1987).
 814 A comparison of four methods for determining planktonic community production.
 815 *Limnology and Oceanography*, 32(5), 1085–1098.
 816 <https://doi.org/10.4319/lo.1987.32.5.1085>

817 Benitez-Nelson, C., Buesseler, K. O., Karl, D. M., & Andrews, J. (2001). A time-series study of
 818 particulate matter export in the North Pacific Subtropical Gyre based on ^{234}Th : ^{238}U
 819 disequilibrium. *Deep-Sea Research Part I: Oceanographic Research Papers*, 48(12), 2595–
 820 2611. [https://doi.org/10.1016/S0967-0637\(01\)00032-2](https://doi.org/10.1016/S0967-0637(01)00032-2)

821 Böttjer, D., Dore, J. E., Karl, D. M., Letelier, R. M., Mahaffey, C., Wilson, S. T., et al. (2017).
 822 Temporal variability of nitrogen fixation and particulate nitrogen export at Station ALOHA.
 823 *Limnology and Oceanography*, 62(1), 200–216. <https://doi.org/10.1002/lno.10386>

824 Boyd, P. W., Claustre, H., Levy, M., Siegel, D. A., & Weber, T. (2019). Multi-faceted particle
 825 pumps drive carbon sequestration in the ocean. *Nature*, 568(7752), 327–335.
 826 <https://doi.org/10.1038/s41586-019-1098-2>

827 de Boyer Montégut, C., Madec, G., Fischer, A. S., Lazar, A., & Iudicone, D. (2004). Mixed layer
 828 depth over the global ocean: An examination of profile data and a profile-based
 829 climatology. *Journal of Geophysical Research: Oceans*, 109(12), 1–20.
 830 <https://doi.org/10.1029/2004JC002378>

831 Brix, H., Gruber, N., Karl, D. M., & Bates, N. R. (2006). On the relationships between primary,
 832 net community, and export production in subtropical gyres. *Deep Sea Research Part II:
 833 Topical Studies in Oceanography*, 53(5–7), 698–717.

834 <https://doi.org/10.1016/j.dsr2.2006.01.024>

835 Buesseler, K. O. (1991). Do upper-ocean sediment traps provide an accurate record of particle
836 flux? *Nature*, 353(6343), 420–423. <https://doi.org/10.1038/353420a0>

837 Buesseler, K. O. (1998). The decoupling of production and particulate export in the surface
838 ocean. *Global Biogeochemical Cycles*, 12(2), 297–310. <https://doi.org/10.1029/97GB03366>

839 Carlson, C. A., Ducklow, H., & Michaels, A. F. (1994). Annual flux of dissolved organic carbon
840 from the euphotic zone in the northwestern Sargasso Sea. *Nature*, 371, 405–408.
841 <https://doi.org/10.1038/371405a0>

842 Cassar, N., Difiore, P. J., Barnett, B. A., Bender, M. L., Bowie, A. R., Tilbrook, B., et al. (2011).
843 The influence of iron and light on net community production in the Subantarctic and Polar
844 Frontal Zones. *Biogeosciences*, 8(2), 227–237. <https://doi.org/10.5194/bg-8-227-2011>

845 Church, M. J., Mahaffey, C., Letelier, R. M., Lukas, R., Zehr, J. P., & Karl, D. M. (2009).
846 Physical forcing of nitrogen fixation and diazotroph community structure in the North
847 Pacific subtropical gyre. *Global Biogeochemical Cycles*, 23, GB2020.
848 <https://doi.org/10.1029/2008GB003418>

849 Church, M. J., Lomas, M. W., & Muller-Karger, F. (2013). Sea change: Charting the course for
850 biogeochemical ocean time-series research in a new millennium. *Deep-Sea Research Part*
851 *II: Topical Studies in Oceanography*, 93, 2–15. <https://doi.org/10.1016/j.dsr2.2013.01.035>

852 Craig, H., & Hayward, T. (1987). Oxygen supersaturation in the ocean: Biological versus
853 physical contributions. *Science*, 235(4785), 199–202.
854 <https://doi.org/10.1126/science.235.4785.199>

855 Dore, J. E., Brum, J. R., Tupas, L. M., & Karl, D. M. (2002). Seasonal and interannual variability
856 in sources of nitrogen supporting export in the oligotrophic subtropical North Pacific
857 Ocean. *Limnology and Oceanography*, 47(6), 1595–1607.
858 <https://doi.org/10.4319/lo.2002.47.6.1595>

859 Duarte, C. M., Regaudie-de-Gioux, A., Arrieta, J. M., Delgado-Huertas, A., & Agustí, S. (2013).
860 The oligotrophic ocean is heterotrophic. *Annual Review of Marine Science*, 5(1), 551–569.

861 <https://doi.org/10.1146/annurev-marine-121211-172337>

862 Ducklow, H. W., & Doney, S. C. (2013). What is the metabolic state of the oligotrophic ocean?
 863 A debate. *Annual Review of Marine Science*, 5(1), 525–533.
 864 <https://doi.org/10.1146/annurev-marine-121211-172331>

865 Emerson, S. (2014). Annual net community production and the biological carbon flux in the
 866 ocean. *Global Biogeochemical Cycles*, 28(1), 14–28.
 867 <https://doi.org/10.1002/2013GB004680>

868 Emerson, S., Quay, P. D., Stump, C., Wilbur, D., & Schudlich, R. (1995). Chemical tracers of
 869 productivity and respiration in the subtropical Pacific Ocean. *Journal of Geophysical*
 870 *Research*, 100(C8), 15873–15887. <https://doi.org/10.1029/95jc01333>

871 Emerson, S., Quay, P. D., Karl, D. M., Winn, C., Tupas, L., & Landry, M. (1997). Experimental
 872 determination of the organic carbon flux from open-ocean surface waters. *Nature*, 389,
 873 951–954. <https://doi.org/10.1038/40111>

874 Emerson, S., Stump, C., & Nicholson, D. P. (2008). Net biological oxygen production in the
 875 ocean: Remote in situ measurements of O₂ and N₂ in surface waters. *Global*
 876 *Biogeochemical Cycles*, 22(3), 1–13. <https://doi.org/10.1029/2007GB003095>

877 Ferrón, S., Wilson, S. T., Martínez-García, S., Quay, P. D., & Karl, D. M. (2015). Metabolic
 878 balance in the mixed layer of the oligotrophic North Pacific Ocean from diel changes in
 879 O₂/Ar saturation ratios. *Geophysical Research Letters*, 42(9), 3421–3430.
 880 <https://doi.org/10.1002/2015GL063555>

881 Ferrón, S., del Valle, D. A., Björkman, K. M., Quay, P. D., Church, M. J., & Karl, D. M. (2016).
 882 Application of membrane inlet mass spectrometry to measure aquatic gross primary
 883 production by the ¹⁸O in vitro method. *Limnology and Oceanography: Methods*, 14(9).
 884 <https://doi.org/10.1002/lom3.10116>

885 Field, C. B., Behrenfeld, M. J., Randerson, J. T., & Falkowski, P. (1998). Primary production of
 886 the biosphere: Integrating terrestrial and oceanic components. *Science*, 281(5374), 237–240.
 887 <https://doi.org/10.1126/science.281.5374.237>

888 García, H. E., & Gordon, L. I. (1992). Oxygen solubility in seawater: Better fitting equations.
889 *Limnology and Oceanography*, 37(6), 1307–1312.
890 <https://doi.org/10.4319/lo.1992.37.6.1307>

891 Giesbrecht, K. E., Hamme, R. C., & Emerson, S. (2012). Biological productivity along Line P in
892 the subarctic northeast Pacific: In situ versus incubation-based methods. *Global*
893 *Biogeochemical Cycles*, 26(3), 1–13. <https://doi.org/10.1029/2012GB004349>

894 Hamme, R. C., & Emerson, S. (2004). The solubility of neon, nitrogen and argon in distilled
895 water and seawater. *Deep-Sea Research Part I: Oceanographic Research Papers*, 51(11),
896 1517–1528. <https://doi.org/10.1016/j.dsr.2004.06.009>

897 Hamme, R. C., & Emerson, S. (2006). Constraining bubble dynamics and mixing with dissolved
898 gases: Implications for productivity measurements by oxygen mass balance. *Journal of*
899 *Marine Research*, 64(1), 73–95. <https://doi.org/10.1357/002224006776412322>

900 Hamme, R. C., Cassar, N., Lance, V. P., Vaillancourt, R. D., Bender, M. L., Strutton, P. G., et al.
901 (2012). Dissolved O₂/Ar and other methods reveal rapid changes in productivity during a
902 Lagrangian experiment in the Southern Ocean. *Journal of Geophysical Research: Oceans*,
903 117(1), 1–19. <https://doi.org/10.1029/2011JC007046>

904 Hannides, C. C. S., Landry, M. R., Benitez-Nelson, C. R., Styles, R. M., Montoya, J. P., & Karl,
905 D. M. (2009). Export stoichiometry and migrant-mediated flux of phosphorus in the North
906 Pacific Subtropical Gyre. *Deep-Sea Research Part I: Oceanographic Research Papers*,
907 56(1), 73–88. <https://doi.org/10.1016/j.dsr.2008.08.003>

908 Haskell, W. Z., Prokopenko, M. G., Stanley, R. H. R., & Knapp, A. N. (2016). Estimates of
909 vertical turbulent mixing used to determine a vertical gradient in net and gross oxygen
910 production in the oligotrophic South Pacific Gyre. *Geophysical Research Letters*, 43(14),
911 7590–7599. <https://doi.org/10.1002/2016GL069523>

912 Hebel, D. V., & Karl, D. M. (2001). Seasonal, interannual and decadal variations in particulate
913 matter concentrations and composition in the subtropical North Pacific Ocean. *Deep-Sea*
914 *Research Part II: Topical Studies in Oceanography*, 48(8–9), 1669–1695.
915 [https://doi.org/10.1016/S0967-0645\(00\)00155-7](https://doi.org/10.1016/S0967-0645(00)00155-7)

916 Juranek, L. W., & Quay, P. D. (2005). In vitro and in situ gross primary and net community
 917 production in the North Pacific Subtropical Gyre using labeled and natural abundance
 918 isotopes of dissolved O₂. *Global Biogeochemical Cycles*, 19(3), 1–15.
 919 <https://doi.org/10.1029/2004GB002384>

920 Juranek, L. W., & Quay, P. D. (2012). Using triple isotopes of dissolved oxygen to evaluate
 921 global marine productivity. *Annual Review of Marine Science*, 5, 503–524.
 922 <https://doi.org/10.1146/annurev-marine-121211-172430>

923 Kaiser, J., Reuer, M. K., Barnett, B., & Bender, M. L. (2005). Marine productivity estimates
 924 from continuous O₂/Ar ratio measurements by membrane inlet mass spectrometry.
 925 *Geophysical Research Letters*, 32(19), 1–5. <https://doi.org/10.1029/2005GL023459>

926 Kana, T. M., Darkangelo, C., Hunt, M. D., Oldham, J. B., Bennett, G. E., & Cornwell, J. C.
 927 (1994). Membrane inlet mass spectrometer for rapid high-precision determination of N₂, O₂,
 928 and Ar in Environmental Water Samples. *Analytical Chemistry*, 66(23), 4166–4170.
 929 <https://doi.org/10.1021/ac00095a009>

930 Kana, T. M., Cornwell, J. C., & Zhong, L. (2006). Determination of denitrification in the
 931 Chesapeake Bay from measurements of N₂ accumulation in bottom water. *Estuaries and*
 932 *Coasts*, 29(2), 222–231. <https://doi.org/10.1007/BF02781991>

933 Karl, D. M. (2014). Solar energy capture and transformation in the sea. *Elementa*, 2, 1–6.
 934 <https://doi.org/10.12952/journal.elementa.000021>

935 Karl, D. M., & Church, M. J. (2014). Microbial oceanography and the Hawaii Ocean Time-series
 936 programme. *Nature Reviews Microbiology*, 12(10), 699–713.
 937 <https://doi.org/10.1038/nrmicro3333>

938 Karl, D. M., & Church, M. J. (2017). Ecosystem structure and dynamics in the North Pacific
 939 Subtropical Gyre: New views of an old ocean. *Ecosystems*, 20(3), 433–457.
 940 <https://doi.org/10.1007/s10021-017-0117-0>

941 Karl, D. M., & Lukas, R. (1996). The Hawaii Ocean Time-series (HOT) program: Background,
 942 rationale and field implementation. *Deep-Sea Research Part II: Topical Studies in*

943 *Oceanography*, 43(2–3), 129–156. [https://doi.org/10.1016/0967-0645\(96\)00005-7](https://doi.org/10.1016/0967-0645(96)00005-7)

944 Karl, D. M., Christian, J. R., Dore, J. E., Hebel, D. V., Letelier, R. M., Tupas, L. M., & Winn, C.
 945 D. (1996). Seasonal and interannual variability in primary production and particle flux at
 946 station ALOHA. *Deep-Sea Research Part II: Topical Studies in Oceanography*, 43(2–3),
 947 539–568. [https://doi.org/10.1016/0967-0645\(96\)00002-1](https://doi.org/10.1016/0967-0645(96)00002-1)

948 Karl, D. M., Hebel, D. V., Björkman, K., & Letelier. (1998). The role of dissolved organic
 949 matter release in the productivity of the oligotrophic North Pacific Ocean. *Limnology and*
 950 *Oceanography*, 43(6), 1270–1286. <https://doi.org/10.4319/lo.1998.43.6.1270>

951 Karl, D. M., Laws, E. A., Morris, P., Williams, P. J. le. B., & Emerson, S. (2003a). Metabolic
 952 balance of the open sea. *Nature*, 426(6962), 32. <https://doi.org/10.1038/426032a>

953 Karl, D. M., Bates, N. R., Emerson, S., Harrison, P. J., Jeandel, C., Llinàs, O., et al. (2003b).
 954 Temporal studies of biogeochemical processes determined from ocean time-series
 955 observations during the JGOFS era. In M. J. R. Fasham (eds) *Ocean Biogeochemistry.*
 956 *Global Change–The IGBP Series*, pp. 239–267. Springer, Berlin, Heidelberg.
 957 https://doi.org/10.1007/978-3-642-55844-3_11

958 Karl, D. M., Church, M. J., Dore, J. E., Letelier, R. M., & Mahaffey, C. (2012). Predictable and
 959 efficient carbon sequestration in the North Pacific Ocean supported by symbiotic nitrogen
 960 fixation. *Proceedings of the National Academy of Sciences of the United States of America*,
 961 109(6), 1842–1849. <https://doi.org/10.1073/pnas.1120312109>

962 Kavanaugh, M. T., Church, M. J., Davis, C. O., Karl, D. M., Letelier, R. M., & Doney, S. C.
 963 (2018). ALOHA from the edge: Reconciling three decades of in situ Eulerian observations
 964 and geographic variability in the North Pacific Subtropical Gyre. *Frontiers in Marine*
 965 *Science*, 5, 130. <https://doi.org/10.3389/fmars.2018.00130>

966 Keeling, C. D., Brix, H., & Gruber, N. (2004). Seasonal and long-term dynamics of the upper
 967 ocean carbon cycle at Station ALOHA near Hawaii. *Global Biogeochemical Cycles*, 18(4),
 968 1–26. <https://doi.org/10.1029/2004GB002227>

969 Laws, E. A. (1991). Photosynthetic quotients, new production and net community production in

970 the open ocean. *Deep-Sea Research*, 38, 143–1617. <https://doi.org/10.1016/0198->
971 0149(91)90059-O

972 Laws, E. A., Landry, M. R., Barber, R. T., Campbell, L., Dickson, M. L., & Marra, J. (2000).
973 Carbon cycling in primary production bottle incubations: Inferences from grazing
974 experiments and photosynthetic studies using ^{14}C and ^{18}O in the Arabian Sea. *Deep-Sea*
975 *Research Part II: Topical Studies in Oceanography*, 47(7–8), 1339–1352.
976 [https://doi.org/10.1016/S0967-0645\(99\)00146-0](https://doi.org/10.1016/S0967-0645(99)00146-0)

977 Laws, E. A., Letelier, R. M., & Karl, D. M. (2014). Estimating the compensation irradiance in
978 the ocean: The importance of accounting for non-photosynthetic uptake of inorganic carbon.
979 *Deep-Sea Research Part I: Oceanographic Research Papers*, 93, 35–40.
980 <https://doi.org/10.1016/j.dsr.2014.07.011>

981 Ledwell, J. R., Watson, A. J., & Law, C. S. (1993). Evidence for slow mixing across the
982 pycnocline from an open-ocean tracer-release experiment. *Letters to Nature*, 364, 701–703.
983 <https://doi.org/10.1038/364701a0>

984 Lee, K. (2001). Global net community production estimated from the annual cycle of surface
985 water total dissolved inorganic carbon. *Limnology and Oceanography*, 46(6), 1287–1297.
986 <https://doi.org/10.4319/lo.2001.46.6.1287>

987 Letelier, R. M., Dore, J. E., Winn, C. D., & Karl, D. M. (1996). Seasonal and interannual
988 variations in photosynthetic carbon assimilation at station ALOHA. *Deep-Sea Research*
989 *Part II: Topical Studies in Oceanography*, 43(2–3), 467–490. <https://doi.org/10.1016/0967->
990 0645(96)00006-9

991 Letelier, R. M., Karl, D. M., Abbott, M. R., & Bidigare, R. R. (2004). Light driven seasonal
992 patterns of chlorophyll and nitrate in the lower euphotic zone of the North Pacific
993 Subtropical Gyre. *Limnology and Oceanography*, 49(2), 508–519.
994 <https://doi.org/10.4319/lo.2004.49.2.0508>

995 Longhurst, A. R., & Harrison, W. G. (1988). Vertical nitrogen flux from the oceanic photic zone
996 by diel migrant zooplankton and nekton. *Deep-Sea Research Part A, Oceanographic*
997 *Research Papers*, 35(6), 881–889. [https://doi.org/10.1016/0198-0149\(88\)90065-9](https://doi.org/10.1016/0198-0149(88)90065-9)

998 Luz, B., & Barkan, E. (2009). Net and gross oxygen production from O₂/Ar, ¹⁷O/ ¹⁶O and
 999 ¹⁸O/¹⁶O ratios. *Aquatic Microbial Ecology*, 56(2–3), 133–145.
 1000 <https://doi.org/10.3354/ame01296>

1001 Marra, J. (2002). Approaches to the measurement of plankton production. In P. J. le. B.
 1002 Williams, D. R. Thomas, & C. S. Reynolds (eds.), *Phytoplankton Productivity and Carbon*
 1003 *Assimilation in Marine and Freshwater Ecosystems*, pp. 222–264. London: Blackwell.

1004 Marra, J. (2009). Net and gross productivity: Weighing in with ¹⁴C. *Aquatic Microbial Ecology*,
 1005 56(2–3), 123–131. <https://doi.org/10.3354/ame01306>

1006 Martínez-García, S., & Karl, D. M. (2015). Microbial respiration in the euphotic zone at Station
 1007 ALOHA. *Limnology and Oceanography*, 60(3), 1039–1050.
 1008 <https://doi.org/10.1002/lno.10072>

1009 Nicholson, D. P., Emerson, S., & Eriksen, C. C. (2008). Net community production in the deep
 1010 euphotic zone of the subtropical North Pacific gyre from glider surveys. *Limnology and*
 1011 *Oceanography*, 53(5), 2226–2236. https://doi.org/10.4319/lo.2008.53.5_part_2.2226

1012 Nicholson, D. P., Stanley, R. H. R., Barkan, E., Karl, D. M., Luz, B., Quay, P. D., & Doney, S.
 1013 C. (2012). Evaluating triple oxygen isotope estimates of gross primary production at the
 1014 Hawaii Ocean Time-series and Bermuda Atlantic Time-series Study sites. *Journal of*
 1015 *Geophysical Research: Oceans*, 117(5), 1–18. <https://doi.org/10.1029/2010JC006856>

1016 Nicholson, D. P., Wilson, S. T., Doney, S. C., & Karl, D. M. (2015). Quantifying subtropical
 1017 North Pacific gyre mixed layer primary productivity from Seaglider observations of diel
 1018 oxygen cycles. *Geophysical Research Letters*, 42(10), 4032–4039.
 1019 <https://doi.org/10.1002/2015GL063065>

1020 Quay, P. D., & Stutsman, J. (2003). Surface layer carbon budget for the subtropical N. Pacific:
 1021 ^δ¹³C constraints at station ALOHA. *Deep-Sea Research Part I: Oceanographic Research*
 1022 *Papers*, 50(9), 1045–1061. [https://doi.org/10.1016/S0967-0637\(03\)00116-X](https://doi.org/10.1016/S0967-0637(03)00116-X)

1023 Quay, P. D., Stutsman, J., Feely, R. A., & Juranek, L. W. (2009). Net community production
 1024 rates across the subtropical and equatorial Pacific Ocean estimated from air-sea ^δ¹³C

disequilibrium. *Global Biogeochemical Cycles*, 23(2), 1–15.
<https://doi.org/10.1029/2008GB003193>

Quay, P. D., Peacock, C., Björkman, K., & Karl, D. M. (2010). Measuring primary production rates in the ocean : Enigmatic results between incubation and non - incubation methods at Station ALOHA. *Global Biogeochemical Cycles*, 24, GB3014.
<https://doi.org/10.1029/2009GB003665>

Reuer, M. K., Barnett, B. A., Bender, M. L., Falkowski, P. G., & Hendricks, M. B. (2007). New estimates of Southern Ocean biological production rates from O₂/Ar ratios and the triple isotope composition of O₂. *Deep-Sea Research Part I: Oceanographic Research Papers*, 54(6), 951–974. <https://doi.org/10.1016/j.dsr.2007.02.007>

Riser, S. C., & Johnson, K. S. (2008). Net production of oxygen in the subtropical ocean. *Nature*, 451(7176), 323–325. <https://doi.org/10.1038/nature06441>

Ryther, J. (1969). Photosynthesis and fish production in the sea. *Science*, 166(7), 72–76.
<https://doi.org/10.1126/science.166.3901.72>

Sadro, S., Nelson, C. E., & Melack, J. M. (2011). Linking diel patterns in community respiration to bacterioplankton in an oligotrophic high-elevation lake. *Limnology and Oceanography*, 56(2), 540–550. <https://doi.org/10.4319/lo.2011.56.2.0540>

Shulenberger, E., & Reid, J. L. (1981). The Pacific shallow oxygen maximum, deep chlorophyll maximum, and primary productivity, reconsidered. *Deep Sea Research Part A, Oceanographic Research Papers*, 28(9), 901–919. [https://doi.org/10.1016/0198-0149\(81\)90009-1](https://doi.org/10.1016/0198-0149(81)90009-1)

Smith, S. D. (1988). Coefficients for sea surface wind stress, heat flux, and wind profiles as a function of wind speed and temperature. *Journal of Geophysical Research: Oceans*, 93(C12), 15467–15472. <https://doi.org/10.1029/JC093iC12p15467>

Sonnerup, R. E., Quay, P. D., & Bullister, J. L. (1999). Thermocline ventilation and oxygen utilization rates in the subtropical North Pacific based on CFC distributions during WOCE. *Deep-Sea Research Part I: Oceanographic Research Papers*.

1052 [https://doi.org/10.1016/S0967-0637\(98\)00092-2](https://doi.org/10.1016/S0967-0637(98)00092-2)

1053 Sonnerup, R. E., Mecking, S., & Bullister, J. L. (2013). Transit time distributions and oxygen
 1054 utilization rates in the Northeast Pacific Ocean from chlorofluorocarbons and sulfur
 1055 hexafluoride. *Deep-Sea Research Part I: Oceanographic Research Papers*, 72, 61–71.
 1056 <https://doi.org/10.1016/j.dsr.2012.10.013>

1057 Sun, O. M., Jayne, S. R., Polzin, K. L., Rahter, B. A., & St Laurent, L. C. (2013). Scaling
 1058 turbulent dissipation in the transition layer. *Journal of Physical Oceanography*, 43(11),
 1059 2475–2489. <https://doi.org/10.1175/JPO-D-13-057.1>

1060 Teeter, L., Hamme, R. C., Ianson, D., & Bianucci, L. (2018). Accurate estimation of net
 1061 community production from O₂/Ar measurements. *Global Biogeochemical Cycles*, 32(8),
 1062 1163–1181. <https://doi.org/10.1029/2017GB005874>

1063 Tortell, P. D., Asher, E. C., Ducklow, H. W., Goldman, J., Dacey, J., Grzyski, J., et al. (2014).
 1064 Metabolic balance of coastal Antarctic waters revealed by autonomous pCO₂ and ΔO₂/Ar
 1065 measurements. *Geophysical Research Letters*, 41, 6803–6810.
 1066 <https://doi.org/10.1002/2014GL061266>

1067 Viviani, D. A., & Church, M. J. (2017). Decoupling between bacterial production and primary
 1068 production over multiple time scales in the North Pacific Subtropical Gyre. *Deep-Sea*
 1069 *Research Part I: Oceanographic Research Papers*, 121, 132–142.
 1070 <https://doi.org/10.1016/j.dsr.2017.01.006>

1071 Volk, T., & Hoffert, M. I. (1985). Ocean carbon pumps: Analysis of relative strengths and
 1072 efficiencies in ocean-driven atmospheric changes. In E. Sundquist & W. S. Broecker (eds.),
 1073 *The carbon cycle and atmospheric CO₂: Natural variations Archean to present*, pp. 99–110,
 1074 American Geophysical Union, Washington, D. C. <https://doi.org/10.1029/GM032p0099>

1075 Wanninkhof, R. (1992). Relationship between wind speed and gas exchange over the ocean.
 1076 *Journal of Geophysical Research*, 97(C5), 7373–7382. <https://doi.org/10.1029/92JC00188>

1077 Wanninkhof, R. (2014). Relationship between wind speed and gas exchange over the ocean
 1078 revisited. *Limnology and Oceanography: Methods*, 12, 351–362.

1079 <https://doi.org/10.4319/lom.2014.12.351>

1080 Weger, H. G., Her-zig, R., Falkowski, P. G., & Turpin, D. H. (1989). Respiratory losses in the
1081 light in a marine diatom: Measurements by short-term mass spectrometry. *Limnology and*
1082 *Oceanography*, 34, 1153–1161. <https://doi.org/10.4319/lo.1989.34.7.1153>

1083 Williams, P. J. le. B. (1993). On the definition of plankton production terms. In W. K. W. Li &
1084 S. Y. Maestrini (eds.) *Measurement of primary production from the molecular to the global*
1085 *scales. ICES marine science symposia*, Volume 197, pp. 9–19. Denmark: International
1086 Council for the Exploration of the Sea.

1087 Williams, P. J. le. B., Morris, P. J., & Karl, D. M. (2004). Net community production and
1088 metabolic balance at the oligotrophic ocean site, station ALOHA. *Deep-Sea Research Part*
1089 *I: Oceanographic Research Papers*, 51(11), 1563–1578.
1090 <https://doi.org/10.1016/j.dsr.2004.07.001>

1091 Williams, P. J. le. B., Quay, P. D., Westberry, T. K., & Behrenfeld, M. J. (2013). The
1092 oligotrophic ocean is autotrophic. *Annual Review of Marine Science*, 5(1), 535–549.
1093 <https://doi.org/10.1146/annurev-marine-121211-172335>

1094 Wilson, J. M., Severson, R., & Beman, J. M. (2014). Ocean-scale patterns in community
1095 respiration rates along continuous transects across the Pacific Ocean. *PLoS ONE*, 9(7),
1096 e99821. <https://doi.org/10.1371/journal.pone.0099821>

1097 Winn, C. D., Campbell, L., Christian, J. R., Letelier, R. M., Hebel, D. V., Dore, J. E., et al.
1098 (1995). Seasonal variability in the phytoplankton community of the North Pacific
1099 Subtropical Gyre. *Global Biogeochemical Cycles*, 9(4), 605–620.
1100 <https://doi.org/10.1029/95GB02149>

1101 Yang, B., Emerson, S., & Bushinsky, S. M. (2017). Annual net community production in the
1102 subtropical Pacific Ocean from in situ oxygen measurements on profiling floats. *Global*
1103 *Biogeochemical Cycles*, 31(4), 728–744. <https://doi.org/10.1002/2016GB005545>

1104 Zhang, H. M., Bates, J. J., & Reynolds, R. W. (2006). Assessment of composite global sampling:
1105 Sea surface wind speed. *Geophysical Research Letters*, 33(17), 1–5.

1106 <https://doi.org/10.1029/2006GL027086>

1107

1108

1109

1110 **Table 1.** Weighted and non-weighted mean GOP and R in mmol O₂ m⁻³ d⁻¹ for different subsets
 1111 of data. The errors are the weighted and non-weighted SD, and for the third column, the
 1112 propagated errors.

	GOP	R	GOP-R
<i>Weighted</i>			
All^a	0.92 ± 0.50	0.83 ± 0.63	0.09 ± 0.29 ^d
p<0.05^b	0.93 ± 0.50	0.83 ± 0.64	0.10 ± 0.30 ^d
p<0.05 & R>0^c	1.00 ± 0.47	0.95 ± 0.56	0.06 ± 0.25 ^d
<i>Non-weighted</i>			
All^a	0.90 ± 0.57	0.67 ± 0.81	0.23 ± 0.99
p<0.05^b	0.92 ± 0.68	0.68 ± 0.86	0.24 ± 1.04
p<0.05 & R>0^c	1.05 ± 0.55	0.91 ± 0.75	0.14 ± 0.93

1113 ^aAll rates included

1114 ^brates from observations with a statistically significant fit to the theoretical O₂ curve

1115 ^crates from observations with a statistically significant fit to the theoretical O₂ curve that did not resulted
 1116 in negative values of R

1117 ^dError propagation takes into account the covariance between GOP and R

1118

1119

Table 2. Annual net community production at Station ALOHA. Top: annual values of NCP for the mixed layer (NCP_{0-mld}) and the entire euphotic zone (0-150 m, NCP_{0-150m}), mixed layer GOP, mixed layer R, ¹⁴C-based primary production (¹⁴C-PP, 0-125m) and particulate C (PC) export at 150m by gravitational sinking. Bottom: flux ratios (\pm propagated SD).

Year	NCP _{0-mld} ^a	NCP _{0-150m} ^b	GOP ^c	R ^c	¹⁴ C-PP ^a	PC flux ^a
		mol O ₂ m ⁻² yr ⁻¹			mol C m ⁻² yr ⁻¹	
2014	2.4 \pm 0.6	2.7 \pm 0.6	24.6 \pm 12.1	23.9 \pm 14.2	19.4 \pm 1.4	0.77 \pm 0.19
2015	2.5 \pm 0.7	2.8 \pm 0.8	22.4 \pm 9.1	18.5 \pm 17.8	18.7 \pm 1.9	1.10 \pm 0.29
2016	2.2 \pm 0.5	2.4 \pm 0.5	13.2 \pm 8.1	9.4 \pm 11.7	17.6 \pm 2.0	0.90 \pm 0.12
2017	2.2 \pm 0.7	2.5 \pm 0.8	11.7 \pm 11.1	7.6 \pm 14.1	17.8 \pm 1.7	0.81 \pm 0.11
2018	1.2 \pm 0.5	1.3 \pm 0.5	12.1 \pm 4.4	10.4 \pm 4.7	14.2 \pm 1.3	0.87 \pm 0.15
2014-18	2.1 \pm 0.6	2.4 \pm 0.6	19.4 \pm 10.4	17.4 \pm 13.4	16.7 \pm 1.5	0.89 \pm 0.16

Year	NCP _{0-mld} /GOP	GOP/ ¹⁴ C ^d	NCP _{0-150m} ^e / ¹⁴ C-PP	PC flux/NCP _{0-150m} ^e
	O ₂ /O ₂	O ₂ /C	C/C	C/C
2014	0.10 \pm 0.05	2.1 \pm 1.1	0.10 \pm 0.03	0.41 \pm 0.14
2015	0.11 \pm 0.05	1.9 \pm 0.8	0.11 \pm 0.03	0.54 \pm 0.21
2016	0.17 \pm 0.11	1.0 \pm 0.6	0.10 \pm 0.02	0.52 \pm 0.13
2017	0.19 \pm 0.19	1.0 \pm 0.0	0.10 \pm 0.03	0.45 \pm 0.15
2018	0.10 \pm 0.05	1.4 \pm 0.5	0.07 \pm 0.03	0.92 \pm 0.39
2014-18	0.11 \pm 0.07	1.7 \pm 1.0	0.10 \pm 0.03	0.53 \pm 0.17

^a annual values calculated by integrating NCP with time using the trapezoidal rule. For individual years, values at the beginning and end of the year were estimated by linear interpolation of rates/fluxes over time. Uncertainties represent the propagated SD for each cruise.

^b Annual NCP_{0-150m} estimated as 1.12 x annual NCP_{mld}

^c annual areal values calculated from weighted annual means (\pm SD) multiplied by average mixed layer depth for each year.

^d mean ¹⁴C-PP for the mixed layer

^e NCP_{0-150m} converted to C units assuming a photosynthetic quotient = 1.4 mol O₂: mol C

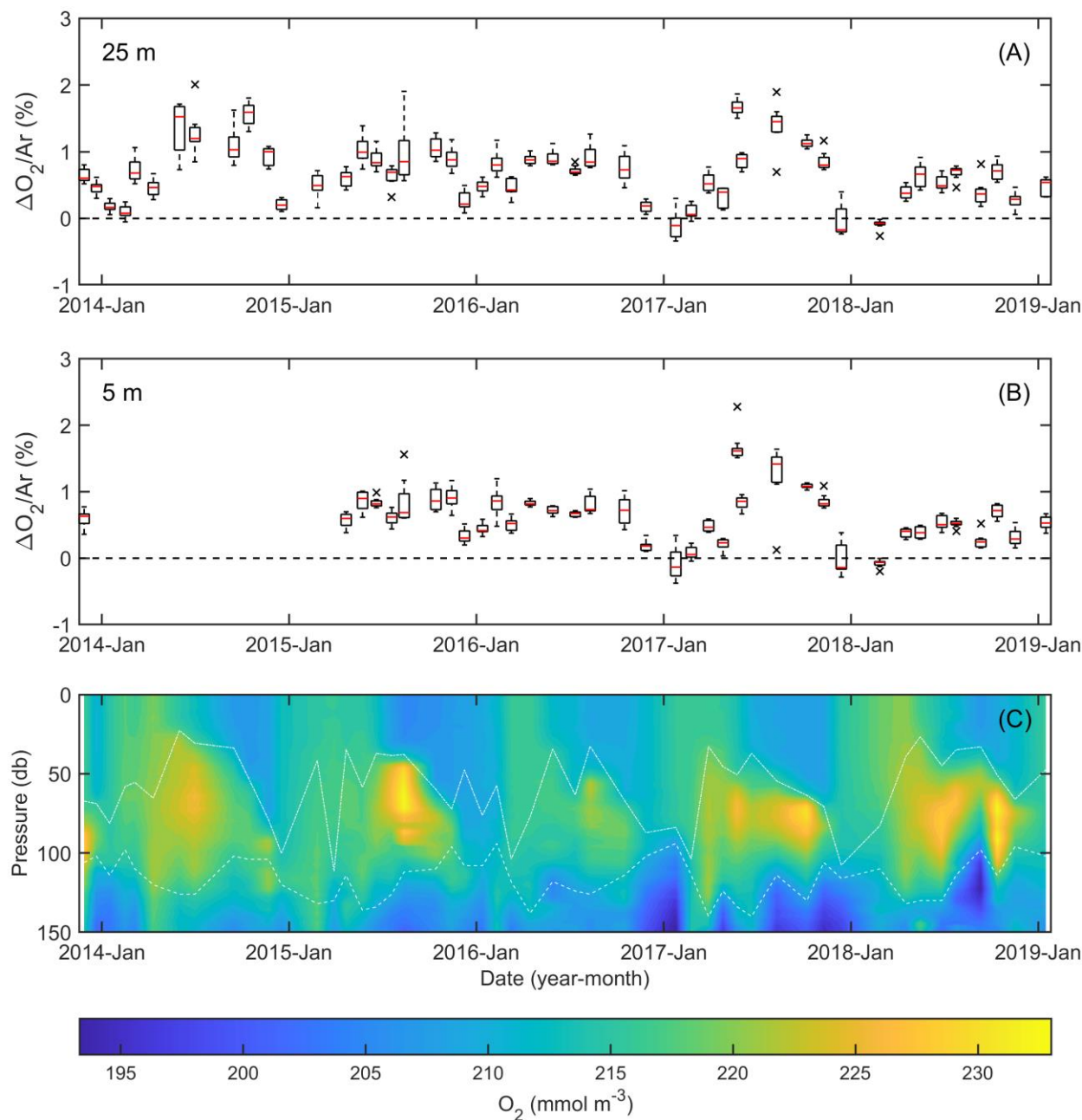
Table 3. Comparison of annual NCP estimates in mol C m⁻² yr⁻¹ in the Subtropical North Pacific, at or in the vicinity of Station ALOHA.

Reference	Method	Time	Depth range	NCP
Brix et al. (2006)	C isotope mass balance	1988-2002	0-150m	3.1 ± 0.3
Emerson et al. (1995)	O ₂ , Ar, N ₂ mass balance	1990	0-100m	1.0 ± 0.7 ^a
Emerson et al. (1997)	O ₂ , Ar, N ₂ mass balance	1990,1992,1995	0-100m	2.7 ± 1.7 ^b
Emerson et al. (2008)	O ₂ , N ₂ mass balance	2004-2005	mixed layer	4.2 ± 1.9 ^c
Hamme & Emerson (2006)	O ₂ , Ar, N ₂ mass balance	2000-2001	~0-115m	1.1 ± 0.5 ^a
Keeling et al. (2004)	C isotope mass balance	1988-2002	mixed layer	2.3 ± 0.8
Lee (2001)	Summertime DIC change	1990	mixed layer	1.7 – 2.2
Quay & Stutsman (2003)	C isotope mass balance	1994-1999	mixed layer	2.3 ± 1.3
Quay et al. (2009)	C isotope mass balance	2004-2005	mixed layer	2.4 ± 1.0 ^a
Quay et al. (2010)	O ₂ , Ar mass balance	2006-2007	mixed layer	3.7 ± 1.0 ^a
Riser & Johnson (2008)	O ₂ mass balance	2002-2005	0-150m	1.6 ± 0.2 ^d
Sonnerup et al. (1999)	CFC-based model	1991	0-100m	2.2 ± 0.5
Sonnerup et al. (2013)	CFC/SF ₆ -based model	2008	winter mixed layer	2.5 – 3.0
Yang et al. (2017)	O ₂ mass balance	2014-2015	winter mixed layer	2.4 ± 0.6 ^c
This study	O ₂ , Ar mass balance	2014-2018	0-150 m	1.7 ± 0.5 ^a

^aConverted to C units using a photosynthetic quotient of 1.4 mol O₂ mol C⁻¹

^bConverted to C units using a photosynthetic quotient of 1.25 mol O₂ mol C⁻¹

^cConverted to C units using a photosynthetic quotient of 1.45 mol O₂ mol C⁻¹



1145

1146

1147

1148

1149

1150

1151

Figure 1. Box and whisker plot of $\Delta O_2/Ar$ measured over a diel cycle at 25 m (A) and 5 m (B) for each cruise during the study period, reflecting the range of variability over a 24-hour period. The red line inside each box is the median, and the bottom and top edges indicate the 25th and 75th percentiles, respectively. The whiskers extend to the most extreme data points, excluding outliers (crosses). (C) Dissolved O_2 as a function of depth and time during the study period.

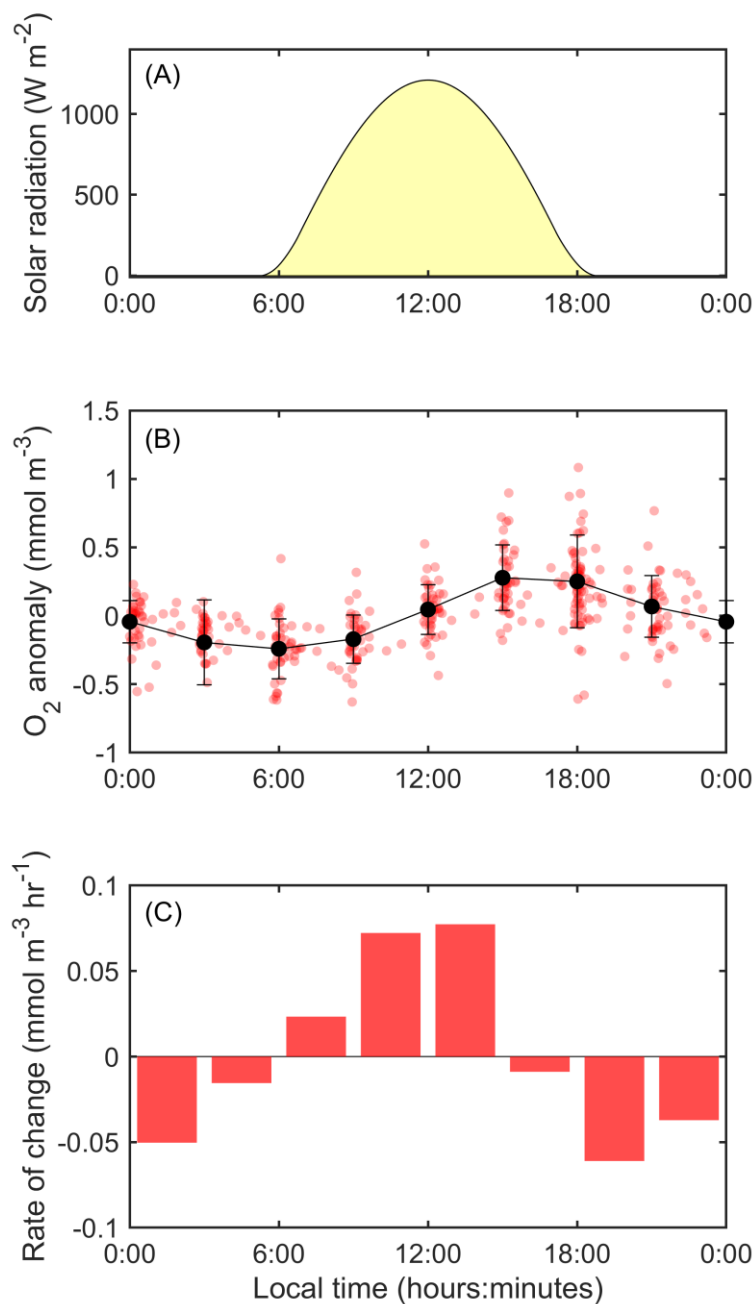
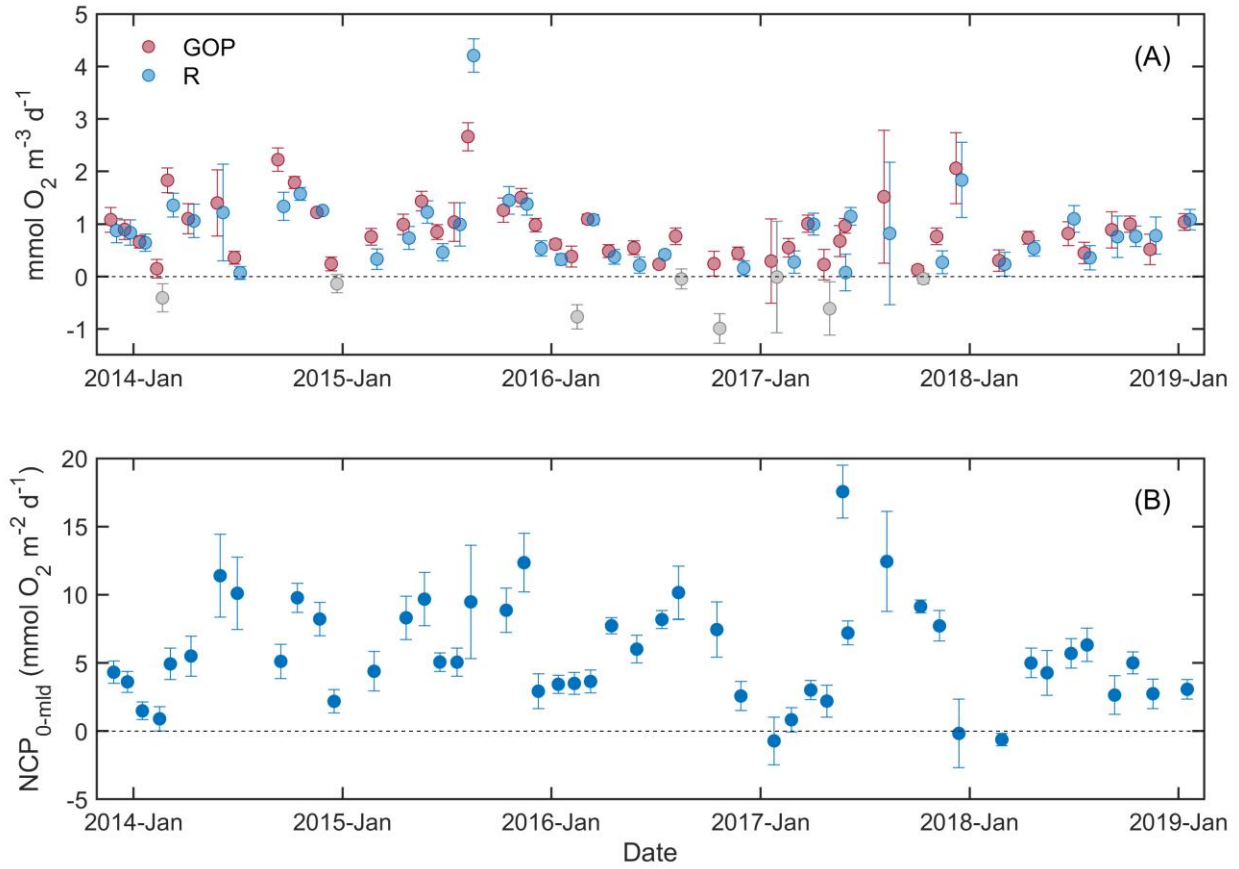
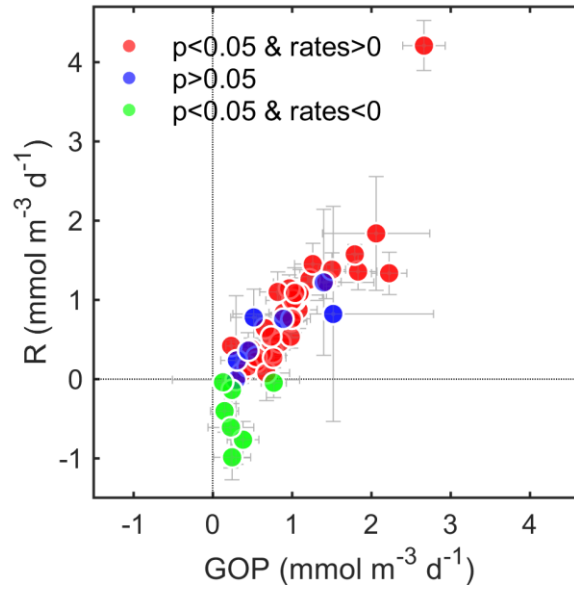


Figure 2. Mean diel cycle of (A) solar irradiance and (B) O_2 anomaly at Station ALOHA in the mixed layer during the study period. Red circles in (B) depict all individual samples, and black circles represent the mean for binned values around the main sampling hours (\pm SD). (C) Rate of change in mean O_2 anomaly as a function of time of the day.



1160

1161 Figure 3. Time series of metabolic rates at Station ALOHA. (A) Volumetric rates of mixed layer
 1162 GOP (red circles) and R (blue circles) derived from diel changes in O_2/Ar . Negative values of R,
 1163 which have no physiological meaning, are depicted as gray circles. Error bars represent fit
 1164 uncertainty, calculated as the SD obtained from bootstrapping the residuals. (B) Areal rates of
 1165 O_2/Ar -based $\text{NCP}_{0\text{-mld}}$. Error bars represent one SD of the mean $\text{NCP}_{0\text{-150m}}$ calculated over a 24-
 1166 hour period.



1167

1168 Figure 4. Rates of GOP and R estimated from the diel changes in $\Delta O_2/Ar$. (A) Scatter plot of
 1169 GOP and R estimated from changes in $\Delta O_2/Ar$ over a 24-hour cycle. Positive rates resulting from
 1170 fits with $p < 0.05$ are depicted as red circles, rates from fits with $p > 0.05$ as blue circles, and
 1171 negative R from fits with $p < 0.05$ as green circles. Error bars represent the fit uncertainty,
 1172 calculated as the SD obtained from bootstrapping the residuals.

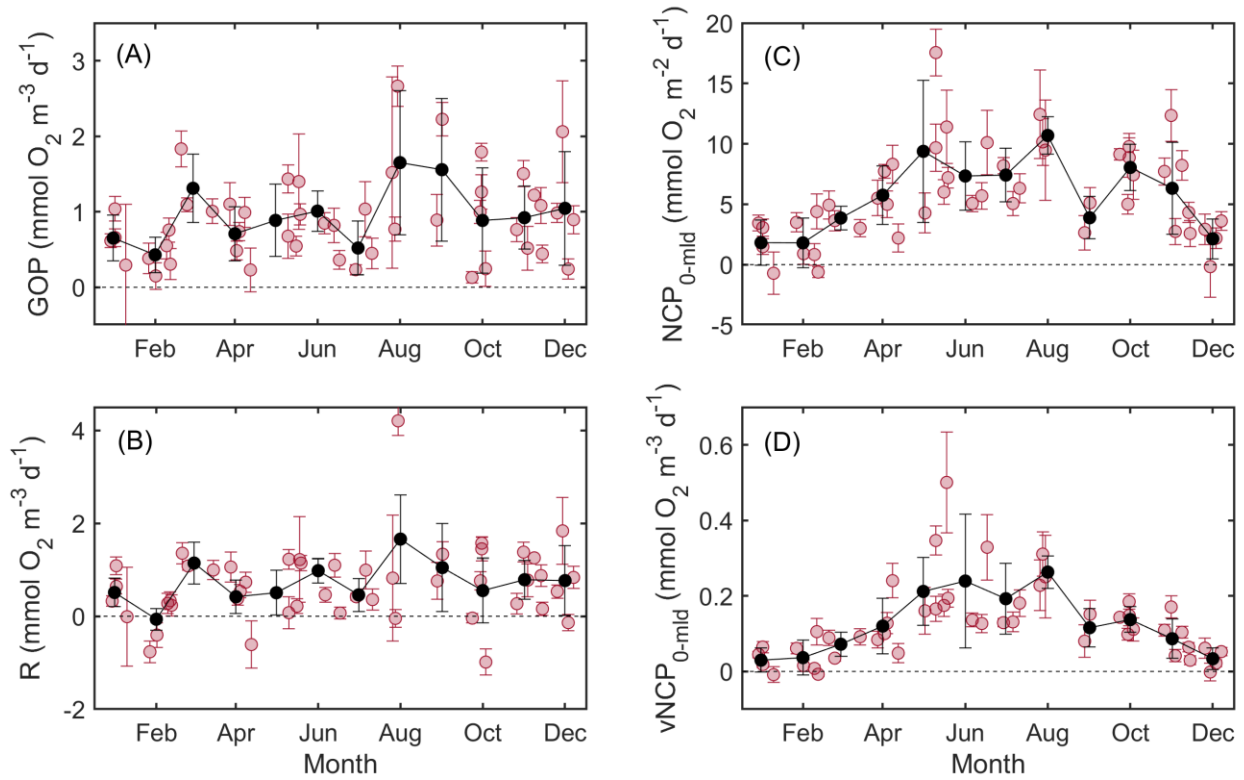
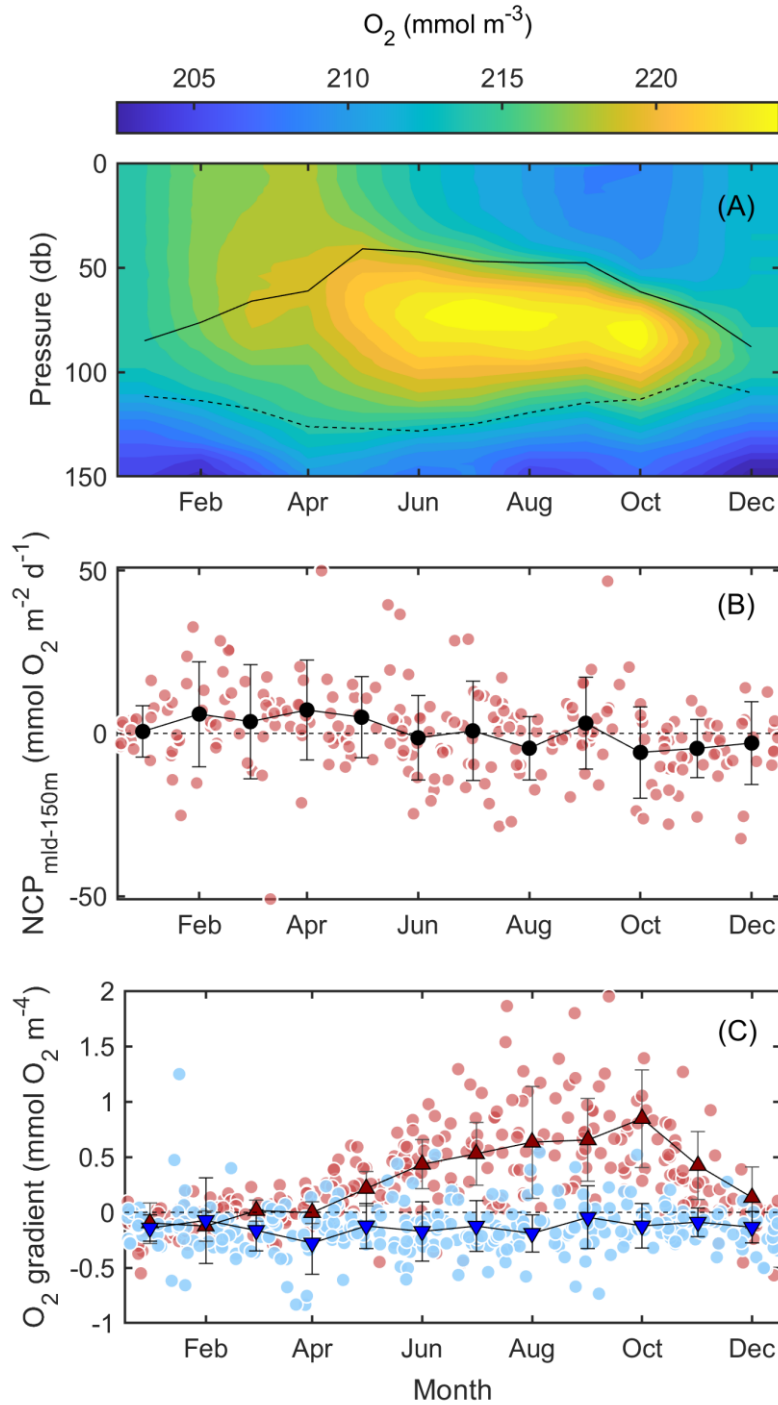


Figure 5. Metabolic rates as a function of time of the year: (A) volumetric GOP, (B) volumetric R, (C) areal NCP_{0-mld}, and (D) vNCP_{0-mld}. Red circles depict all observations. Red error bars in (A) and (B) represent the error in the individual fits, whereas in (C) and (D) they represent the SD over a 24-hour cycle. Black circles depict the mean for each month (\pm SD).



1180

1181 Figure 6. (A) Monthly climatology of dissolved O_2 in the upper 150m at Station ALOHA. Black
 1182 solid and dashed lines depict the mixed layer depth and DCM, respectively. (B) Estimates of
 1183 month to month $NCP_{\text{mld-150m}}$ at Station ALOHA. Red circles depict all individual estimates
 1184 during the HOT time-series, and black circles represent the monthly mean values (\pm SD). (C) O_2
 1185 gradients at the base of the mixed layer (red circles) and at 150 m (blue circles). Negative values
 1186 indicate decreasing dissolved O_2 concentration with depth. Red and blue triangles represent the

monthly mean in the O_2 gradients at the base of the mixed layer and the DCM, respectively, with the error bars showing 1SD of the mean.

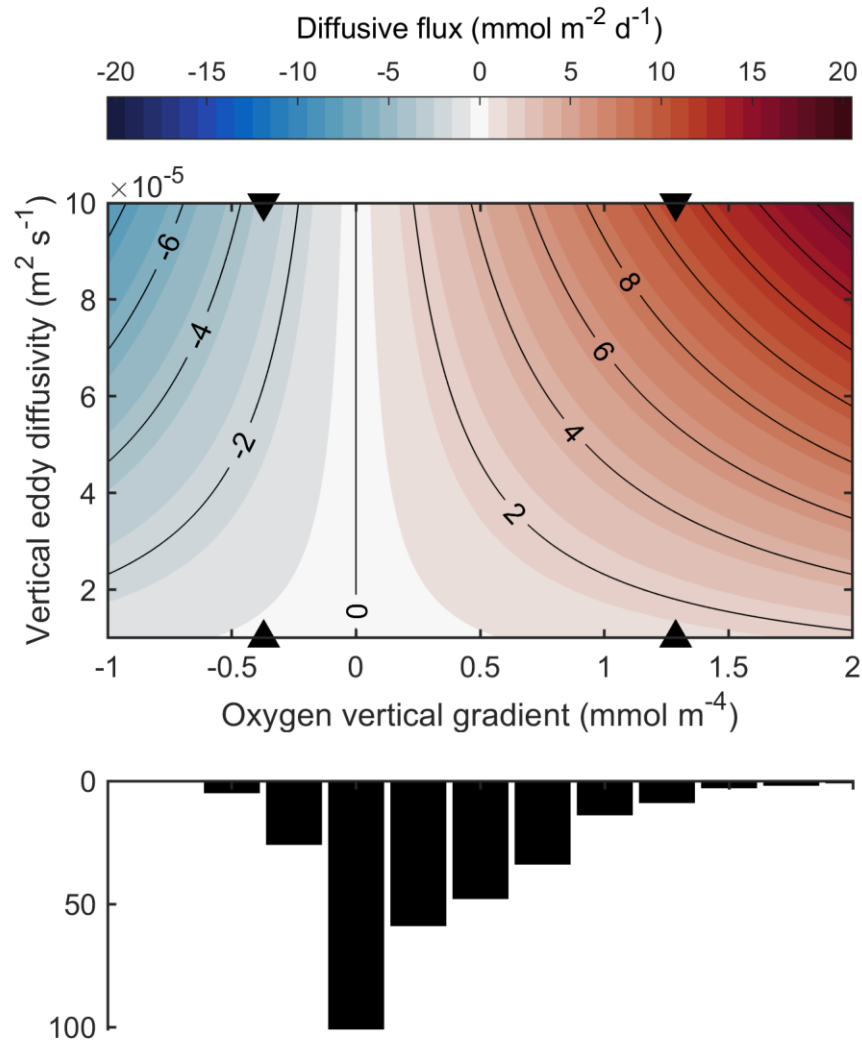
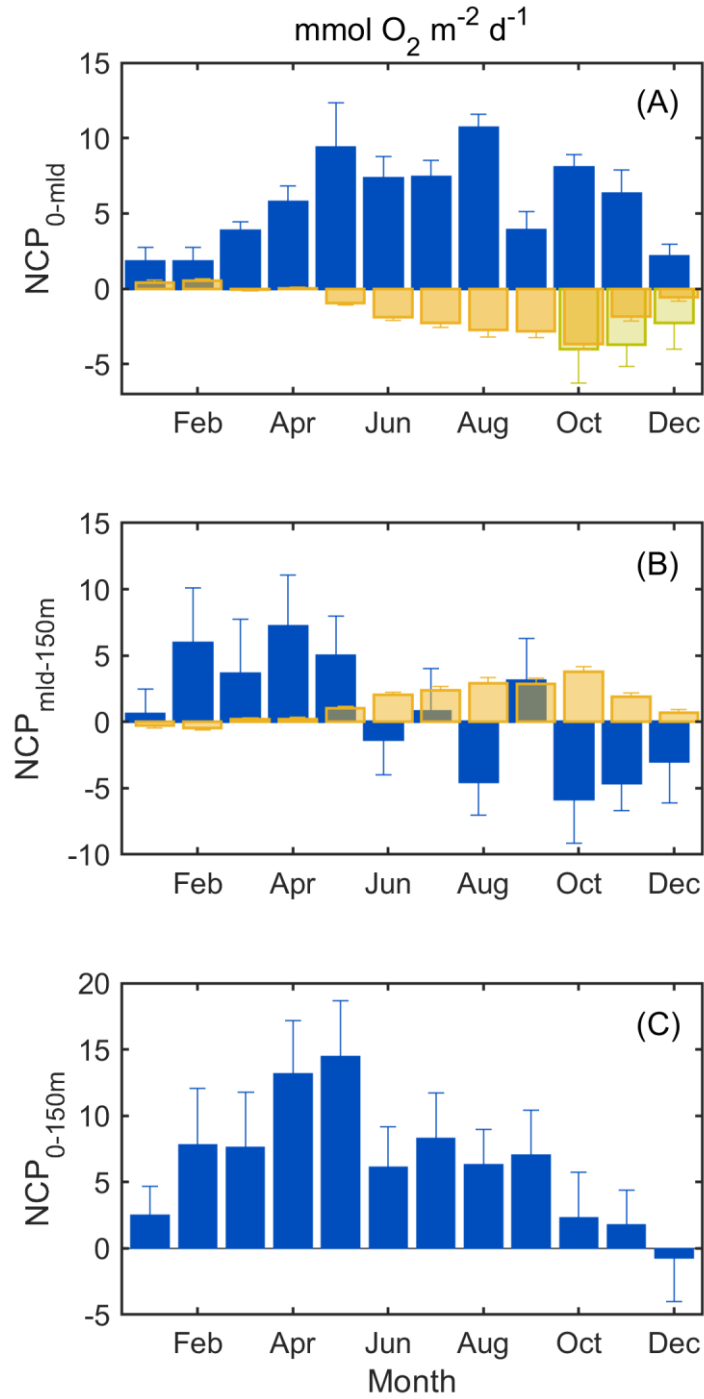


Figure 7. Sensitivity of the diapycnal flux of O_2 at the base of the mixed layer to changes in vertical O_2 gradients and K_z . The triangles on the x axis encompass 95.5% of the measured vertical gradients. The bottom histogram shows the distribution of vertical O_2 gradients measured between January 1996 and January 2019.



1196

1197 Figure 8. Monthly NCP means: (A) Uncorrected O_2/Ar -derived NCP in the mixed layer ($\text{NCP}_{0\text{-mld}}$, dark blue bars), estimated NCP flux correction due to diapycnal O_2 fluxes at the base of the
 1198 mixed layer (orange bars, calculated using a K_z of $0.5 \times 10^{-4} \text{ m}^2 \text{ s}^{-1}$), and estimated flux
 1199 correction due to entrainment (green bars). Error bars denote the standard error (SE). (B)
 1200 Uncorrected NCP for the lower euphotic zone ($\text{NCP}_{\text{mld-150m}}$, dark blue bars) and estimated NCP
 1201 flux correction due to both vertical O_2 fluxes at the base of the mixed layer and at 150m
 1202

1203 (calculated using a K_z of $0.1 \times 10^{-4} \text{ m}^2 \text{ s}^{-1}$) (orange bars). Error bars denote 1SE. (C) Total NCP
1204 in the euphotic zone ($\text{NCP}_{0-150\text{m}}$), calculated by adding uncorrected NCP_{mld} plus uncorrected
1205 $\text{NCP}_{\text{mld}-150\text{m}}$ minus the flux of O_2 across 150 m. Note that by adding NCP_{mld} and $\text{NCP}_{\text{mld}-150\text{m}}$
1206 there is no need to correct for the flux across the base of the mixed layer. The errorbars show the
1207 propagated SE. In (A) and (B) positive NCP correction fluxes are out of the layer (would need to
1208 be added to NCP values to correct for O_2 vertical fluxes), and vice versa.